Final Report

Project 22 – 006
Hydrogen Cyanide for Improved Identification of Fire Plumes in the $(BC)^2$ Network

Prepared for
Texas Air Quality Research Program (AQRP)
The University of Texas at Austin

Prepared by

Dr. Tara I. Yacovitch (PI) and Conner Daube
Aerodyne Research, Inc.

Dr. Rebecca Sheesley and Dr. Sascha Usenko, Co-PIs
Baylor University

8/31/2023
Version 2

QA Requirements: Technical Systems Audits - Not Required for the Project
Audits of Data Quality – 10% Required
Report of Findings – Required in Final Report

Table of Contents

List of Figures

List of Acronyms

AAE – Absorption Ångström Exponent
AQRP – Air Quality Research Program
ARI – Aerodyne Research, Inc.
BB – Biomass Burning
BC – Black Carbon
$(BC)^2$ – Black and Brown Carbon $(BC)^2$ study
BrC – Brown Carbon
BU – Baylor University
C_2H_2 – Acetylene aka ethyne
C_2H_6 – Ethane
CH_4 – Methane
CO – Carbon Monoxide
CO_2 – Carbon Dioxide
DFW – Dallas-Fort Worth
DQI – Data Quality Indicator
H_2O – water vapor
HCN – Hydrogen Cyanide
IR – Infrared
NASA – National Aeronautics and Space Administration
NCAR – National Center for Atmospheric Research
NO_2 – Nitrogen dioxide
NOAA – National Oceanic and Atmospheric Administration
NOx – Oxides of nitrogen
PI – Principal Investigator
PM – Particulate Matter
PM_{org} – Particulate Matter organics, or organic aerosol
PMF – Positive Matrix Factorization
PTR-MS – Proton transfer reaction mass spectrometer
QA – Quality Assurance
QAPP – Quality Assurance Project Plan
QC – Quality control
RS-232 – Recommended standard 232, a serial communication standard
SAE – Scattering Ångström Exponent
sccm – standard cubic centimeters per minute
SLPM – standard liters per minute
SP-AMS – Soot-Particle Aerosol Mass Spectrometer
TCEQ – Texas Commission on Environmental Quality
TCP-IP – Transmission Control Protocol/Internet Protocol
TILDAS – Tunable Infrared Laser Direct Absorption Spectrometer or Spectroscopy
US EPA – United States Environmental Protection Agency
UZA – ultra-zero air

Executive Summary

Wildfire incidents in the US have and will continue to increase with a changing climate. Smoke can impact the local air quality in Texas from both local/in-state fires, and transported emissions from other parts of the US and from Mexico. The 2020 Black and Brown Carbon $(BC)^2$ study demonstrated how wavelength-dependent aerosol optical properties could be used to track the influence of biomass burning (BB). The $(BC)^2$ network operated in El Paso, Houston and Galveston in 2020 -21 and has been expanded to include Dallas-Fort Worth in 2023.

Hydrogen cyanide (HCN) is a small nitrogen-containing molecule produced by BB, and in limited quantities from vehicle combustion. This project aims to improve smoke plume characterization with the addition of HCN to the $(BC)^2$ network. This goal addresses AQRP's 2022-2023 research priorities, notably "Domestic Fire Emissions" and Performing this monitoring at a Dallas-Fort-Worth site ties in with the AQRP's 2022-2023 research priority "Changing Emission Patterns in Texas."

HCN was integrated into a new $(BC)^2$ network trailer at TCEQ's "Fort Worth Northwest" site. Measurements were conducted from April 6th, 2023 and ending July 6th, 2023. HCN quality assurance is complete. Advanced analysis focuses on the identification of BB events through a series of case studies. Recommendations for future work are included.

We observe that both the Absorbing Angstrom Exponent (AAE), a proxy for brown carbon contribution to aerosol absorption, and the absorption coefficient, a proxy for the total smoke loading in the atmosphere, must be elevated before noticeable enhancements in HCN are observed. Thus, when HCN is elevated, biomass burning emissions are more likely to have an impact on local air quality.

We have identified several short-duration spikes with HCN:CO ratios indicative of traffic. However, we do not conclusively identify any broad/regional traffic-only HCN plumes. Certain broad HCN-only plumes without associated enhancements in AAE were investigated, and HCN/CO ratios for these plumes fall within the range of expected values for biomass burning. The poor HCN/CO correlations however suggest plumes of mixed origin, and back-trajectory investigations indicate that the airmasses transited regions of heavy rainfall, potentially washing out the aerosols.

During the 3-week Dallas Field Study (AQRP Project 22-010), the HCN measurement agrees with a positive matrix factorization analysis of the organic aerosol measured by the Soot Particle Aerosol Mass Spectrometer, and identifies a BB event that had an AAE enhancement just above the threshold, but with a strong enhancement in the absorption coefficient. The reason may be that this event consisted of an aerosol plume of mixed origin (BB organic aerosol comprised 20% of the total organic aerosol mass). At other times, the absence of HCN suggests certain identified peaks are *not* of BB origin or have a very low aerosol absorption coefficient.

Through this project, HCN is shown to be a high-sensitivity BB tracer even in this urban environment.

1.0 Introduction

Wildfire activity has and will continue to increase with changing climate [*Abatzoglou and Williams*, 2016; *Westerling et al.*, 2006]. US wildfires in the Western US produce more particulate matter (PM) pollution than all other US aerosol sources combined [*Liu et al.*, 2017] and they promote widespread, substantial regional increases in ozone (O_3) [*Jaffe et al.*, 2013; *Selimovic et al.*, 2020]. The risks of wildfires in Texas are also increasing due to dry conditions and fuel load [*Nielsen-Gammon et al.*, 2021]. Emissions from wildfires and agricultural burning have the potential to impact Texas' air quality. Sources of smoke observed in Texas originate both from within the state and from sources in Mexico or other parts of the US.

The Black and Brown Carbon $(BC)^2$ 2019-21 study was designed to identify the influence of wildfires and dust events on urban air quality in Texas. The central indicator of biomass burning and dust impact at the $(BC)^2$ sites is the Ångström exponent. The Absorption Ångström Exponent (AAE) is used to track the influence of biomass burning through the quantification of the wavelength dependence of the aerosol absorption. Biomass burning aerosol has a strong wavelength dependence which results in an AAE >>1, while fossil combustion from motor vehicles has little wavelength dependence and an AAE ~1. The Scattering Ångström Exponent (SAE) is used to track the influence of dust through the quantification of the wavelength dependence of aerosol scattering. Larger particles have an SAE approaching zero while smaller particles have an enhanced SAE. The AAE and the SAE are monitored in real time to characterize the influence of wildfires and dust on urban air quality in Texas.

The $(BC)^2$ monitoring network in 2020-21 included four monitoring trailers which were deployed adjacent to existing TCEQ sites in the Houston metropolitan area and in El Paso (Figure 1). The Houston sites were Galveston, West Liberty/Liberty and Aldine. The El Paso site was at the University of Texas at El Paso (UTEP). For this monitoring year, the El Paso site was moved to accommodate growth on the UTEP campus, and two additional sites were set up in Dallas/Fort Worth. The network nominally operates annually during the ozone season (Apr – Oct, funding permitting).

Identification of biomass burning (BB) smoke influence using aerosol optical measurements has been demonstrated to be effective for a variety of locations and conditions, however, measurement of both gas and particle tracers will improve characterization of the chemistry of the smoke plume, thereby improving understanding of BB contribution to gas and particle phase air quality within urban areas.

The goal of this project is thus to improve smoke plume characterization with the addition of hydrogen cyanide (HCN), a gas-phase fire tracer, to the $(BC)^2$ smoke monitoring network. HCN is a small nitrogen-containing molecule produced in significant quantities from biomass burning [*Hayden et al.*, 2022], and in limited quantities from vehicle combustion [*Moussa et al.*, 2016; *Wren et al.*, 2018]. This pilot

project will set the stage for future potential expansions of the $(BC)^2$ network monitoring capabilities across the state.

This goal explicitly addresses the AQRP's 2022-2023 research priorities, notably "Domestic Fire Emissions" including transported emissions from wildfires (domestic, international) and their impacts on exceptional events in Texas. Performing this monitoring at a Dallas-Fort Worth - Northwest site ties in with the AQRP's 2022-2023 research priority "Changing Emission Patterns in Texas", which includes additional research along the Interstate-35.

The new Dallas-Fort Worth site at the TCEQ-operated CAMS site "Fort Worth Northwest" (32.8058182, -97.3565229) was set up as part of the TCEQ-funded $(BC)^2$ network expansion. The HCN monitor installed in the $(BC)^2$ network trailer, for measurements conducted in spring/summer 2023.

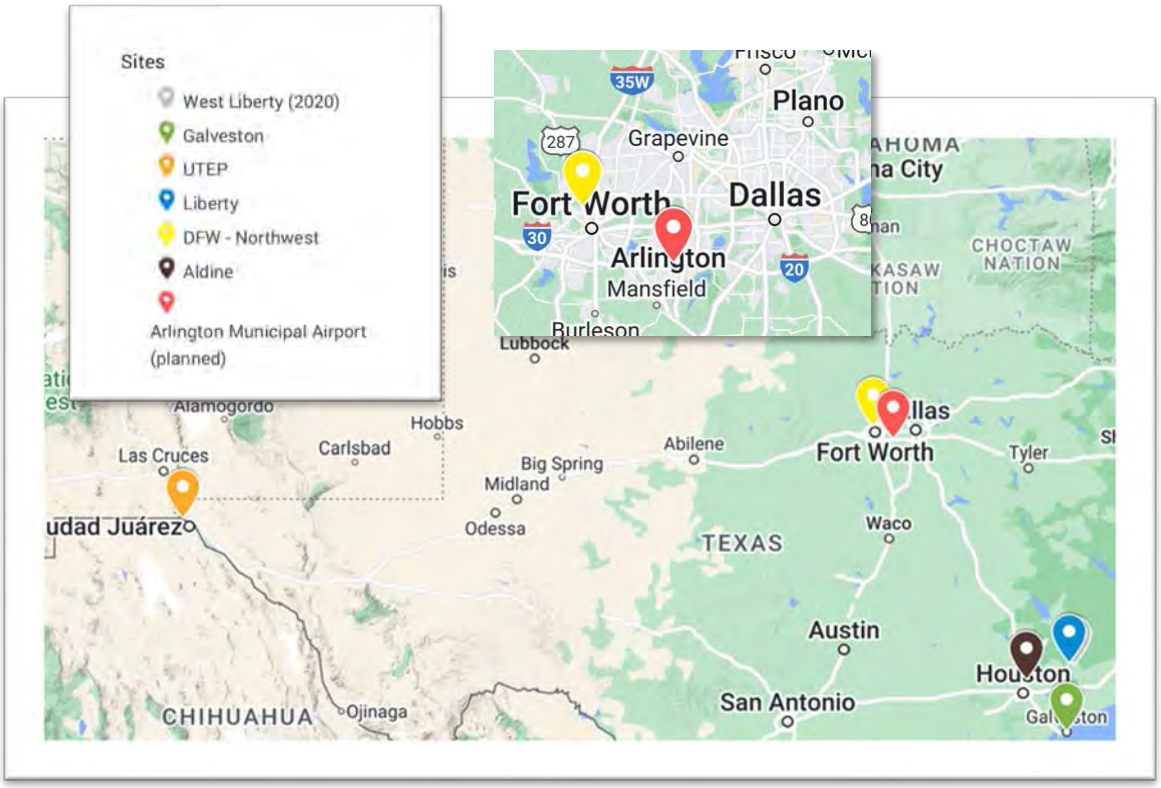

Figure 1. Map of 2020-22 $(BC)^2$ network. The HCN measurement and associated $(BC)^2$ measurements will be at the DFW – Northwest site.

This project is divided into 4 tasks:

1. Design Measurement Campaign: site choice, logistics, campaign planning
2. Execute Field Campaign: HCN measurements at the chosen Dallas Fort-Worth site

3. HCN Data Analysis: Quality assurance of the HCN dataset
4. Fire Plume Data Analysis: Enhanced identification of biomass burning plumes using HCN data to enhance existing $(BC)^2$ network data.

2.0 Methods

2.1 Hydrogen Cyanide Instrument

The target analyte of this project is hydrogen cyanide, HCN. The measurement relies on tunable infrared (IR) spectroscopy of the 3287 cm^{-1} absorption of HCN (Figure 2). Additional species are present in this in the wavelength window and must be fit for accurate retrieval of HCN. These species are water vapor and acetylene (C_2H_2). In the raw measurement dataset, HCN, H_2O and C_2H_2 will be reported as uncalibrated raw mixing ratios, with accuracies determined by their spectral lines as present in the HITRAN database [*Gordon et al.*, 2017] (typically accurate to <10%). In the final dataset, HCN data will be further corrected calibrated using results from a dedicated calibration tank. Other collected TILDAS data will be used for quality assurance (QA) but not produced as deliverables, including ambient temperature, instrument cell pressure, and laser light level.

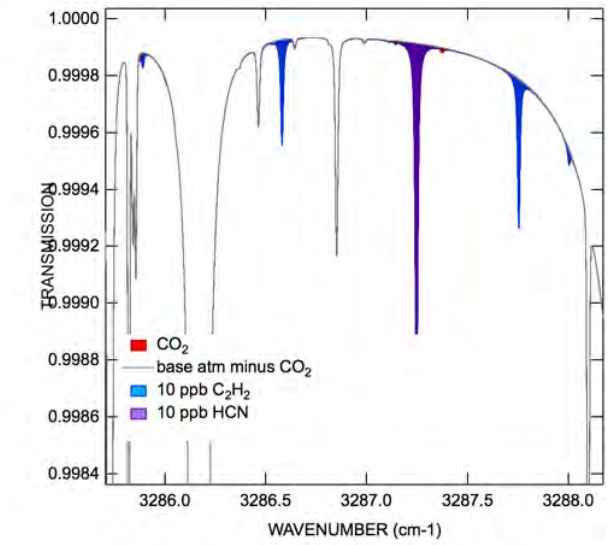

Figure 2. Spectral window for the TILDAS measurement of HCN (purple). Acetylene (C_2H_2, blue) and water are also present in this spectral region.

A miniature Tunable Infrared Direct Absorption Spectrometer (mini-TILDAS)[*McManus et al.*, 2015; *Warneke et al.*, 2023] provides a continuous measurement of HCN. The instrument reports data at 1 Hz, with regular (hourly) but brief (<1 min) interruptions for auto backgrounds, which serve to minimize long-term baseline drift.

Figure 3. Picture (left, instrument top off) of the Aerodyne mini-TILDAS HCN monitor.

Numerous other measurements, which are not covered in the scope of work of this project, will be collected at the Dallas-Fort Worth $(BC)^2$ site.

2.2 Integration into the $(BC)^2$ network trailer

During the week of October 24 – 28, 2023, the HCN instrument was installed into a rackmount case in the $(BC)^2$ network trailer at Baylor University (Figure 4). A thermoelectric chiller designed to maintain stable and precise temperatures for the laser and optics housing was connected to the instrument. A dry scroll vacuum pump was used to flow ambient air through the sample cell (~5.5 SLPM). Sample tubing (1/2" PFA) was run from the instrument to a filtered inlet at the top of the trailer. Near the inlet tip, another line of tubing was connected perpendicular into the sample line and run to an ultra-zero air (UZA) compressed gas cylinder in the trailer (Figure 5). Every hour, a valve would trigger release of UZA in excess of the sample flow for a minute to "overblow" the sample inlet and enable the instrument software to calculate a background (via a spectral baseline). Equipment was secured to the floor and wall using straps and metal plates.

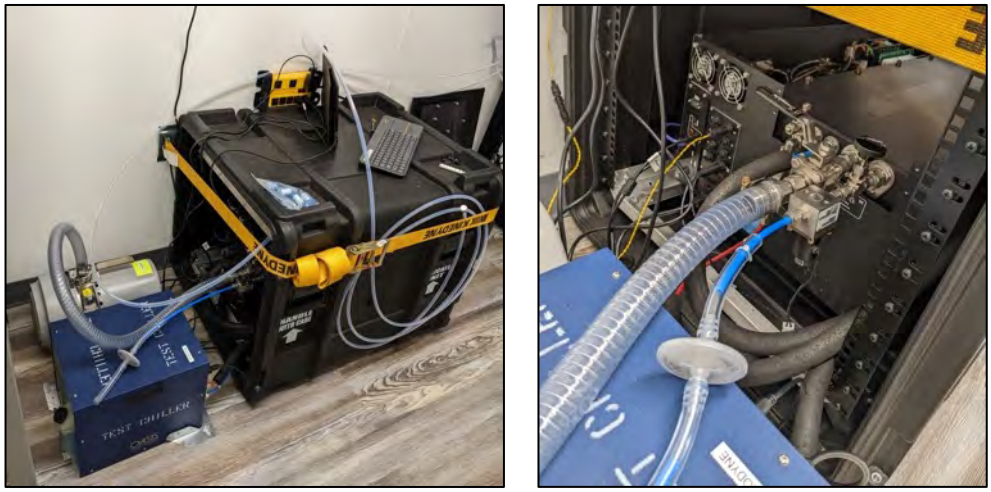

Figure 4. Instrument installed in a rackmount case in the $(BC)^2$ network trailer (left picture). Close-up of connections at the back of the instrument for pumping, fluids, valve control, power, and networking (right picture).

Figure 5. Sampling inlet (middle) near other sampling ports and equipment (left picture). Sampling inlet (close-up) with filter and zero air delivery line.

After the initial turn-on, there was a period of optical optimization (i.e., mirror alignment) and electrical testing of various components (detector, NI cards, TEC board). A calibration was performed by diluting various small volumes of an HCN standard into the UZA overblow line. Test data was collected in this configuration for approximately a month. Due to an issue with the detector and certain valve control, the instrument was removed from the rackmount case and shipped back to Aerodyne on December 14th, 2023. During troubleshooting of the instrument at Aerodyne, a contact issue on a data acquisition card connector was found to be the cause of the faulty valve behavior. Testing at Aerodyne continued for a period of months, including a biomass burning experiment that verified the reformed performance of the instrument. The instrument was transported to the testing region aboard the Aerodyne Mobile Laboratory on April 2nd.

Figure 6. The Aerodyne Mobile Laboratory at Fort Worth Meacham International Airport parked next to the $(BC)^2$ network trailer.

On April 6th, the HCN TILDAS was integrated into the $(BC)^2$ network trailer located at Fort Worth Meacham International Airport (Figure 6). After several days of thermal equilibration, the instrument exhibited similar noise to laboratory testing back at Aerodyne (< 70 ppt in 1 s). On April 14th, gas cylinders were delivered to enable regular background zeroing procedures. A calibration was performed on April 22nd by Aerodyne personnel using a standard previously used for calibrations at Baylor in November 2022. On April 10th, the Aerodyne Mobile Laboratory (AML) arrived at Mecham International Airport to conduct measurements as part of a concurrent field campaign (AQRP 22-010). While parked stationary at night between April 10th and April 23rd, the AML also gathered auxiliary data (species such as CO, HCN, and various VOCs).

2.3 Aerosol optical measurements

2.3.1 Realtime aerosol inlet

The real-time aerosol absorption and scattering instrumentation sampled off a $PM_{2.5}$ cyclone inlet which operated at 16.7 lpm. Flow was controlled after each instrument using a mass flow controller. A 90-mm quartz fiber filter was in front each mass flow controller to prevent clogging. These mass flow controllers were monitored remotely via DAQ Factory.

Figure 7. Left: Side view of the instrumentation and high-volume aerosol sampler. Right: Two tricolor absorption photometers (TAPs) and a nephelometer

2.3.2 Optical Absorption Measurements – Tricolor Absorption Photometer

A tricolor absorption photometer (TAP; Model 2901, Brechtel Inc., Hayward, CA) was used to measure the aerosol light absorption coefficients (σ_{abs}) at UV (365 nm), green, (520 nm) and red (640 nm) wavelengths. The TAP is the commercially available version

of NOAA's continuous light absorption photometer (CLAP) and uses 10 solenoid valves to consecutively sample through eight sample filter spots and two reference filter spots [*Ogren et al.*, 2017]. LED light sources simultaneously shine light through the sample and reference spots. The reference spot allows a differential measurement approach in the TAP so the increase in light attenuation due to deposited particles on the sample spot can be largely separated from filter effects. A transmittance threshold for light attenuation was set to 50% to change the sampling filter spot. Each of the 8 sample spots is separated from the other by O-rings that clamp the filter material to prevent any inter-spot leakage. The air flow passes through the filter and into a solenoid valve controlled by the TAP Reader software. For spot loading effect, TAP automatically does the correction using its inbuilt methodology (based on the filter correction method discussed by Ogren., [2010]) and the instrument output is real-time, corrected absorption coefficients. The TAPs measure σ_{abs} every second which is averaged to 5-minute data. TAP data acquisition is performed using the TAP software provided by Brechtel.

2.3.3 Optical Scattering Measurements – Nephelometer

Aerosol scattering coefficients (σ_{scat}) at three different wavelengths (450 blue, 525 green and 635 red) were measured using an Ecotech Aurora 3000 nephelometer. Ecotech Aurora 3000 nephelometer uses a white light source to illuminate the air sample and the light scattered by the aerosol particles (and gases) at a particular wavelength is measured using a photomultiplier tube. In addition, this nephelometer provides a separate measurement of particle back-scatter (σ_{bscat}). The instrument automatically calculates Rayleigh scattering from internally measured temperature and pressure and corrects the reported signal for those factors. Calibration of the nephelometer was performed prior to the instrument being set up at the site and then every 15 days using CO_2 as a span gas. Zero checks are performed once every week by using internally filtered particle-free air passed through High Efficiency Particulate Air (HEPA) filter. The chamber temperature inside the nephelometer was set to 40^{o} C. This helped to maintain a relative humidity (RH) <40% for scattering measurements as per the GAW recommendations [*GAW*, 2011]. Scattering measurements are corrected for angular truncation errors following the procedure described by Müller et al. [2011]. Averaging time was set to a five-minute average. Nephelometer data acquisition is performed using the DAQFactory software.

2.3.4 Calculated aerosol optical properties

Ångström Exponents Calculations

The TAP and nephelometer measurements were used to calculate the Ångström (Absorption and Scattering) exponents for characterization of the wavelength dependency of aerosol absorption and scattering, respectively. The Ångström exponent is calculated as the negative slope of the linear fit of the optical parameter versus the wavelengths on a log-log plot [*Moosmüller and Chakrabarty*, 2011]. The Ångström

exponents for three wavelength bands can be represented using the following equation [*Bergstrom et al.*, 2007; *Kirchstetter et al.*, 2004; *Schnaiter et al.*, 2006; *Schnaiter et al.*, 2005].

$$\text{Absorption Ångström Exponent} = -\frac{\log\left(\sigma abs_{\lambda 1,}\, \sigma abs_{\lambda 2,}\, \sigma abs_{\lambda 3,}\right)}{\log(\lambda 1, \lambda 2, \lambda 3)} \quad (1)$$

The absorption Ångström exponent (AAE) is calculated with the absorption coefficient data measured using the TAPs at 640, 520, 365 nm (λ_1, λ_2, and λ_3, respectively). The SAE is calculated with the scattering coefficient measured using the nephelometer at 450, 525 and 635 nm (λ_1, λ_2, and λ_3, respectively).

$$\text{Scattering Angstrom Exponent} = -\frac{\log\left(\sigma scat_{\lambda 1,}\, \sigma scat_{\lambda 2,}\, \sigma scat_{\lambda 3,}\right)}{\log(\lambda 1, \lambda 2, \lambda 3)} \quad (2)$$

SAE is an intrinsic property of the aerosol derived based on the wavelength dependency of the aerosol scattering. SAE is inversely related to the particle size which indicates that larger particles will have smaller SAE and vice-versa [*Schmeisser et al.*, 2017].

2.4 Biomass Burning Plume Identification Algorithm

One of the goals of this project is to identify and characterize fire events impacting the Dallas/Fort Worth. As the project is connected to/co-located with the TCEQ $(BC)^2$ project (2021 campaign final report for TCEQ PGA: 582-21-22317-016), we use the same methodology to identify periods of biomass burning influence. The campaign AAE average and standard deviations are used to define the baseline by location. The project defines a biomass burning event as a deviation from the site baseline as follows:

1. AAE > site average + 1 standard deviation
2. Duration of enhanced AAE
    a. Long BB: > 4 hr enhanced AAE
    b. Short BB: 1-4 hr enhanced AAE
    c. Local plume: <1 hr enhanced AAE
3. SAE > 1

By using the site average, we also are allowing for different baseline conditions for aerosol optical properties at different sites. The time limitation and the SAE limitation were included after preliminary analysis of AAE using all datapoints and an SAE cutoff of 1.0. As AAE from BB can vary due to combustion conditions and atmospheric processing, an absolute threshold is difficult to define and may result in biased assignment of BB influence.

For this project we are considering different durations of BB event periods. Since we are evaluating the integration of HCN with aerosol optical properties (AOP), we are not only

interested in long range transport, but in better understanding each of these BB tracers. The Long BB category is the duration used by $(BC)^2$ networks to identify long range transport BB. The Short BB category is designed to identify BB events that may be more closer range BB events and/or lower influence events that do not remain above the threshold. The Local plume category is designed to identify whether the combined HCN + AOP protocol can confirm the BB sourcing for short duration plumes that may have local origins. To further characterize each event period, we will include the average absorption coefficient, back trajectory analysis using NOAA HYSPLIT and remote sensing products (e.g. NOAA Hazard Mapping System Fire and Smoke product https://www.ospo.noaa.gov/Products/land/hms.html#maps).

All data for identified BB events are included in Appendix B Tables 1-3.

2.5 Audit of Data Quality

A data quality audit on 10 % of the generated time-series is required. We focus on one trace from the instrument (HCN, with C_2H_2 and H_2O also produced), and will include the entire time period of interest. In practice, with only 3 traces to produce, we plot all traces during this exercise for 100% data coverage.

The data audit is done by plotting the selected time series along with data from other projects (the Baylor-led $(BC)^2$ network expansion data; the mobile laboratory data from AQRP 22-010; TCEQ-acquired meteorological parameters) for diagnostic tracers.

An overview of the HCN time series is shown below. 1-second data is in green, with 5-minute average data overlaid in black. We observe many brief spikes, and sections of elevated background. Auxiliary tracers are also shown: acetylene, C_2H_2 and water, H_2O, from the HCN instrument; CO from the Aerodyne Mobile Lab, collocated with the site, and from the $(BC)^2$ network trailer; wind speed (pale blue) and direction (red) from the TCEQ trailer at the Fort Worth Northwest site. Blue vertical shading indicates times when the mobile lab from project AQRP 22-010 was co-located with the site. These times will have a second measurement of HCN, as well as numerous other volatile organic hydrocarbon and particulate matter measurements.

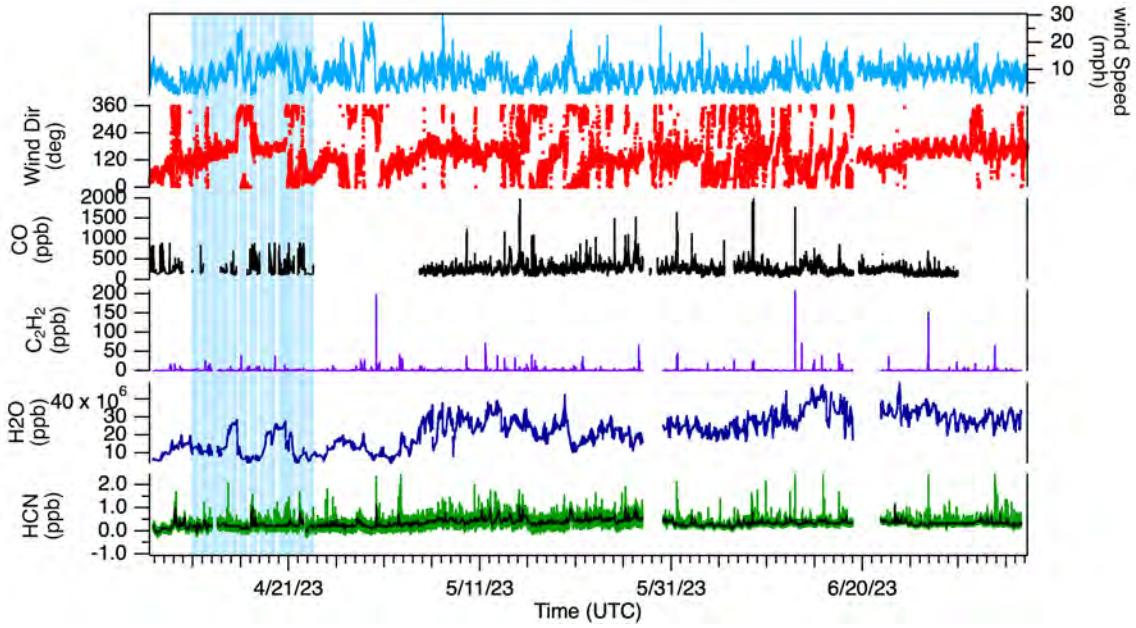

Figure 8. Overview of HCN time series, with 1-second data shown in green, and a 5-minute average overlaid in black. Auxiliary tracers are also shown: acetylene, C_2H_2 and water, H_2O, from the HCN instrument; CO from the collocated mobile lab and the $(BC)^2$ network trailer; and wind speed (pale blue) and direction (red) from the TCEQ trailer at the Fort Worth Northwest site. Blue vertical shading indicates times when the mobile lab from project AQRP 22-010 was co-located with the site.

The following data quality indicators were assessed:

- *Zeroes or calibration periods present:* *None present*
- *Glitches showing unphysical mixing ratios:* *None present*
- *Biases in data versus reference (if available):* *Pending**
- *Instrument noise performance:* *Acceptable, see below*
- *Missing times:* *2 times, See below*
- *Other data quality issues:* *No zeroes, see below*

*A comparison of the HCN data measured during this project will be done with the HCN data measured by the AML. HCN data from that project is not yet calibrated.

2.5.1 HCN performance

The instrument performance during the campaign is assessed using a period of ambient data with no major HCN plumes. An appropriate data section is shown below. This section of data is from early in the campaign, and shows an acceptable performance of 1-second, 1-sigma noise of 78 ppt, versus a data quality metric of 80 ppt. Later on in the campaign, after a power outage, the performance improves slightly.

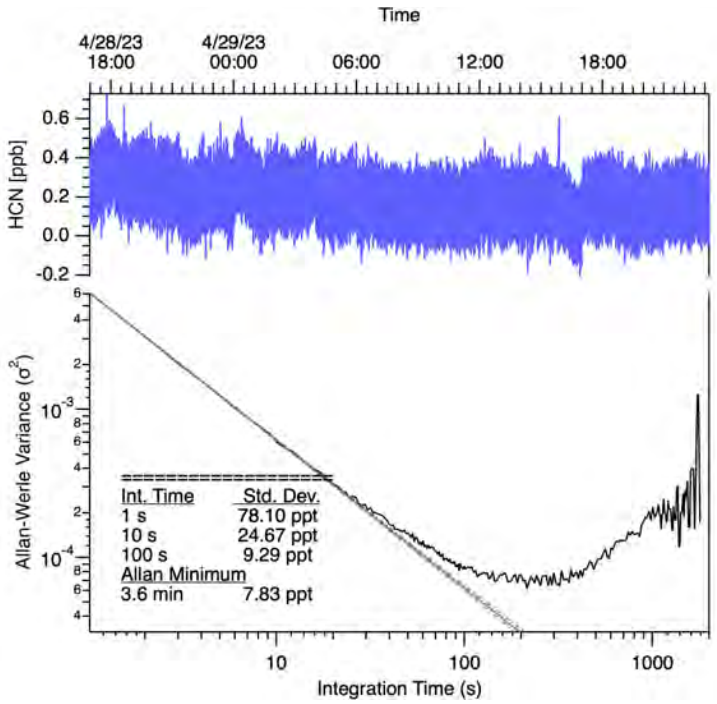

Figure 9. Typical performance of the HCN monitor showing 1-second noise of 78 ppt. Performance is deemed acceptable if 1-second noise is < 80 ppt.

2.5.2 No Autobackgrounding/Zeroing

There were two major periods when no autobackground gas was being delivered to the instrument, and as a result, the instrument was run without ABG. This manifests itself as a small offset in reported mixing ratios. In the graph below, the grey trace is the raw HCN mixing ratio, with the green trace corrected for this offset. The first period requiring offset correction occurs at the beginning of the campaign, due to delays in delivery of Ultra Zero Air to the site. The second period occurs around 5/31 and is due to a failure of the autobackgrounds after recovering from a power outage. The offset correction leverages spectral refitting and archival spectral data (see QA document) to fit the same type of spectra with a consistent set of fit parameters. This is especially important for the correction of the first offset period, where there is a small data gap before zeroes are begun.

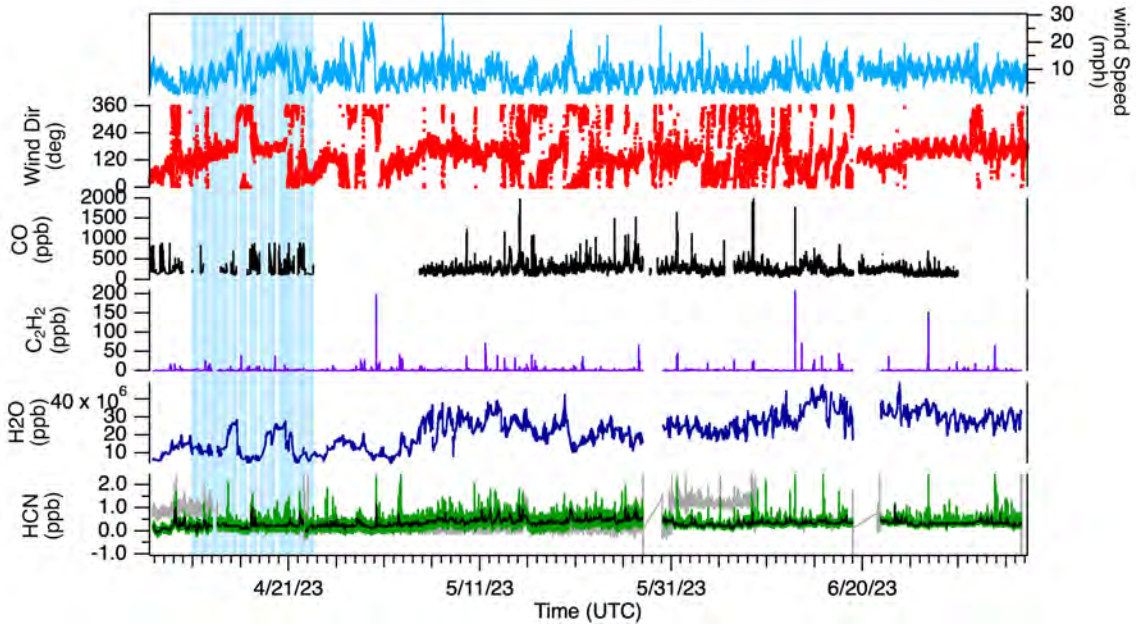

Figure 10. Full HCN time series showing raw (grey) and QA'ed (green) HCN data. There are two periods when an offset correction was needed.

2.5.3 Data Gaps

Two data gaps have been identified in the HCN data trace. These gaps are attributed to power loss at the site, based on the absence of data from other measurements at the site. The HCN instrument recovery lagged power restoration at the site. There was also typically a short period of data after instrument re-start that needed to be excised due to unphysical mixing ratios prior to zeroing.

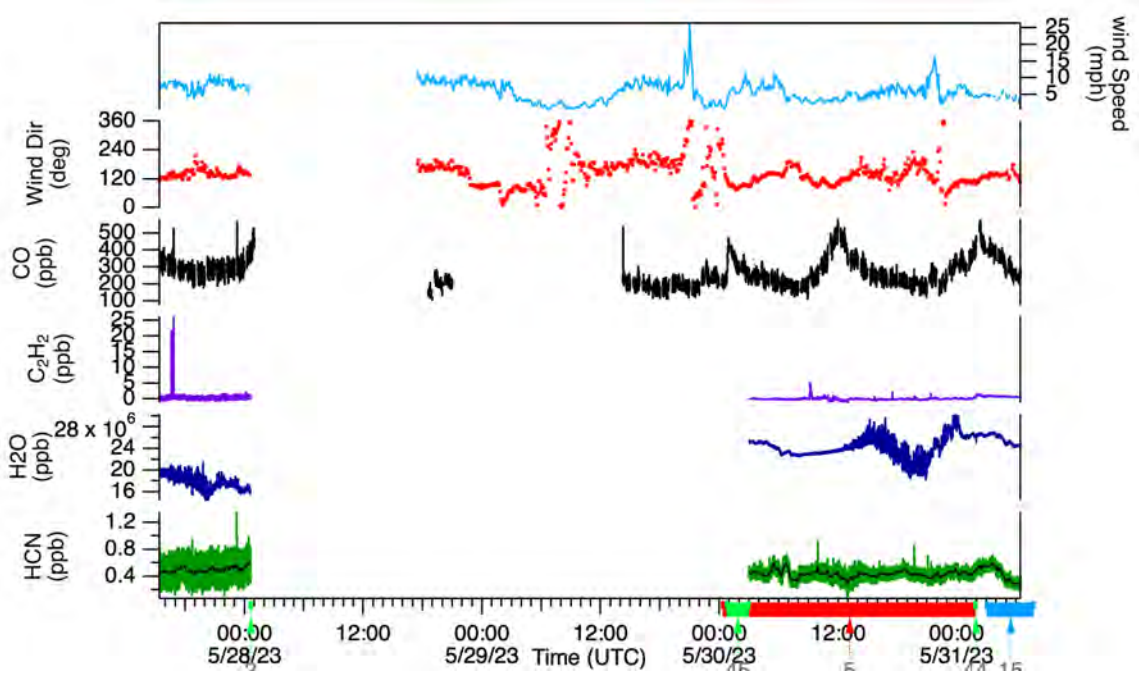

Figure 11. First HCN data gap beginning on 5/28/23 UTC. The wind data (blue, red) are from the TCEQ Fort Worth Northwest site. The CO data (black) are from the (BC)2 project. The HCN (green, with black 5 min average), C_2H_2 (purple) and H_2O (navy blue) data are from this project.

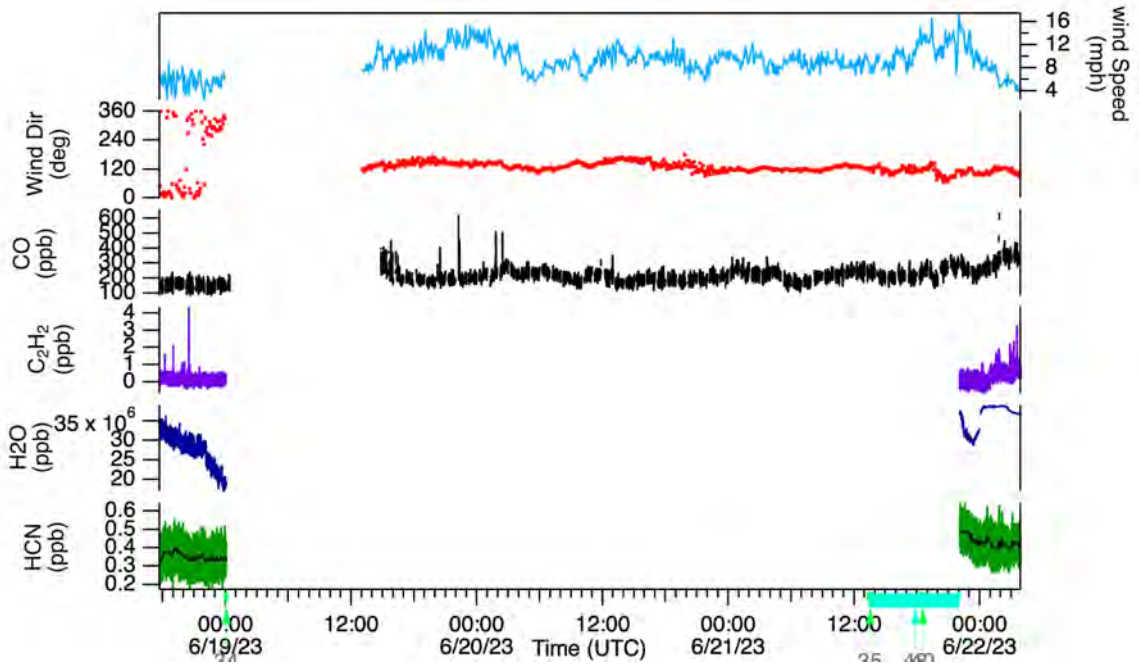

Figure 12. Second HCN data gap beginning on 6/19/23 UTC. The wind data (blue, red) are from the TCEQ Fort Worth Northwest site. The CO data (black) are from the (BC)2 project. The HCN (green, with black 5 min average), C_2H_2 (purple) and H_2O (navy blue) data are from this project.

3.0 Results and Discussion

3.1 HCN Measurements at Fort Worth Northwest

HCN measurements at the Fort Worth Northwest site were conducted in spring/summer 2023. The campaign ran from 4/6/23 20:31 UTC to 7/6/23 13:58 UTC, which includes 83 measurement days (data gaps are not counted), exceeding the 66 measurement days originally proposed. A summary HCN time series is shown below, with fast 1-second data (green) and 5-minute average data (black) shown.

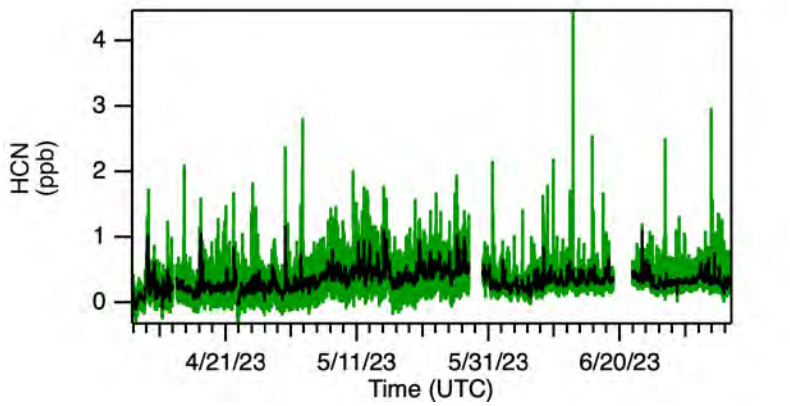

Figure 13. Overview of HCN measurements performed at the Fort Worth Northwest site.

The average mixing ratio is 0.33 ppb, with maximum mixing ratios of 4.46 ppb during a brief spike. Many spikes are apparent upon first glance. In fact, these spikes are a combination of rapid plumes we attribute to local traffic, and slower plumes that are more likely to be of regional origin.

We focus in on a few interesting time periods. First, the largest magnitude measurement of 4.46 ppb. This period consists of real plumes, though they are brief. Coincident enhancements in acetylene (C_2H_2) and CO (black) suggest a nearby traffic source. This particular time period will be filtered out in the following section.

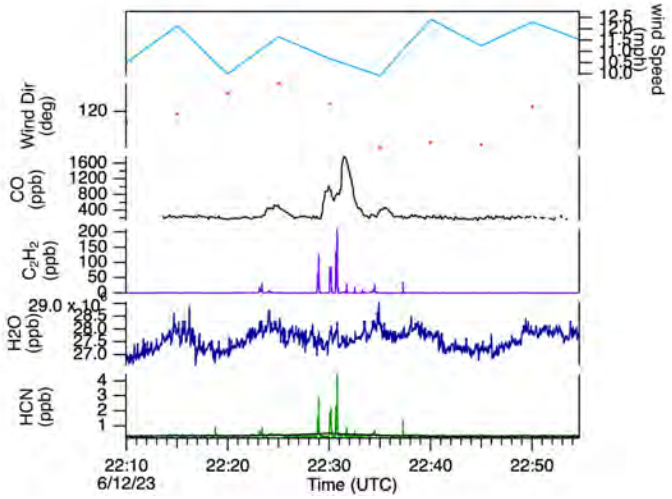

Figure 14. Measurement period showing the highest HCN mixing ratio.

Next, we focus on a period between 4/8 and 4/11/2023, showing significantly broader enhancements. The HCN mixing ratio rises from a background level of about 0.3 to up to 1 ppb. This period occurred at a time of suspected smoke measurement, and is investigated in the BB event discussion below.

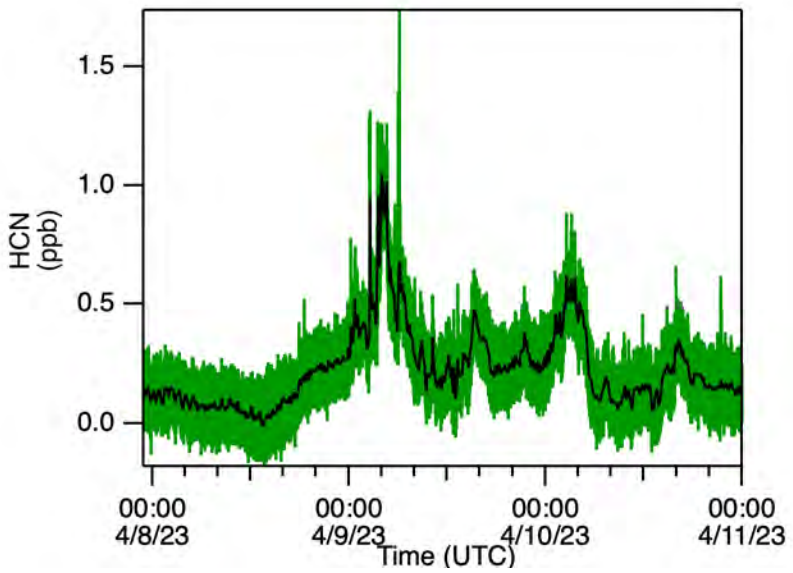

Figure 15. Measurement period showing broad enhancements in HCN mixing ratio. CST = UTC – 6h

3.2 Traffic Filtering

Short-duration spikes in HCN are ubiquitous in the HCN dataset. Though HCN serves as an excellent biomass burning tracer, it is also present in other source types, notably vehicle exhaust emissions [*Moussa et al.*, 2016]. We investigate filtering out of some of these short duration spikes in two ways. First, we consider only the time duration of spikes, flagging and filtering out short duration spikes. Next, we investigate the ratio of HCN to other tracers to see if there are consistent ratios in these suspected local exhaust interferences. Then, this ratio can be investigated in broader HCN enhancements as another diagnostic metric.

Filtering by duration: Extremely short-duration HCN plumes are assumed to be traffic-related, and can be filtered based on their duration. We determine the minimum HCN concentration in a given 10-second time window. We then calculate the difference between HCN and this minimum, yielding a delta HCN trace. We choose a threshold of 0.6 ppb as a cutoff in the delta HCN trace to indicate a “spike”. This threshold is chosen to balance spike detection but not flag measurements in the noise band of the instrument. In Figure 16, we compare the QA’ed HCN time trace (thick pale green trace) with the filtered trace with no spikes (deep green). This procedure succeeds in excising short-duration spikes, keeping the longer-duration HCN enhancement visible around 5/20/23 12:00 UTC. Figure 17 shows how this filtering works on > 4 ppb HCN peak discussed in the previous section.

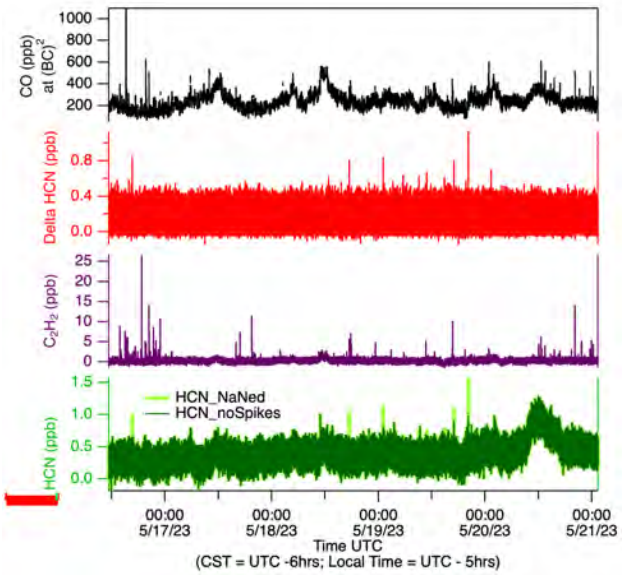

Figure 16. Example time period showing filtered spikes (pale green) and the no-spikes data (deep green). Other auxiliary tracers are shown (CO and C_2H_2). Delta HCN (red), an intermediate measurement used in this filtering, is also shown.

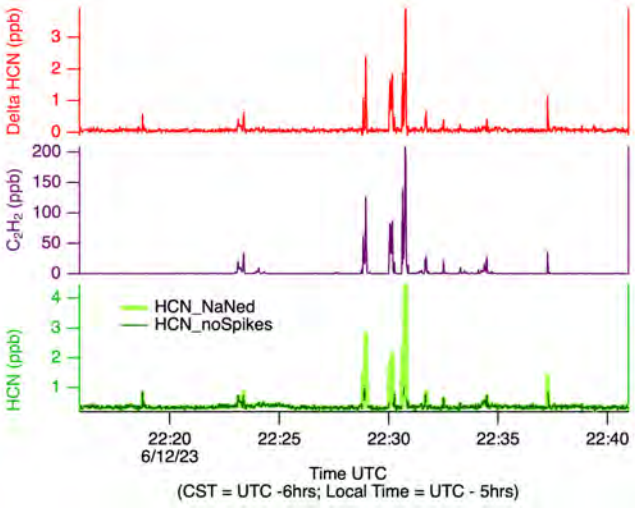

Figure 17. Filtering of the high-mixing ratio spike >4 ppb.

Next, we investigate ratios of tracers during the short-duration and longer-duration events. Below, the HCN mixing ratio is colored by HCN/C_2H_2 ratio, with ratios of 0-1 shown. Since HCN and C_2H_2 are measured in the same instrument, and background ratios of these tracers are near-zero, the direct ratio of HCN/C_2H_2 at a given time is taken. We see a fair bit of variability in the molar ratios for the filtered spikes in this period. We note that the longer duration enhancement does not contain C_2H_2.

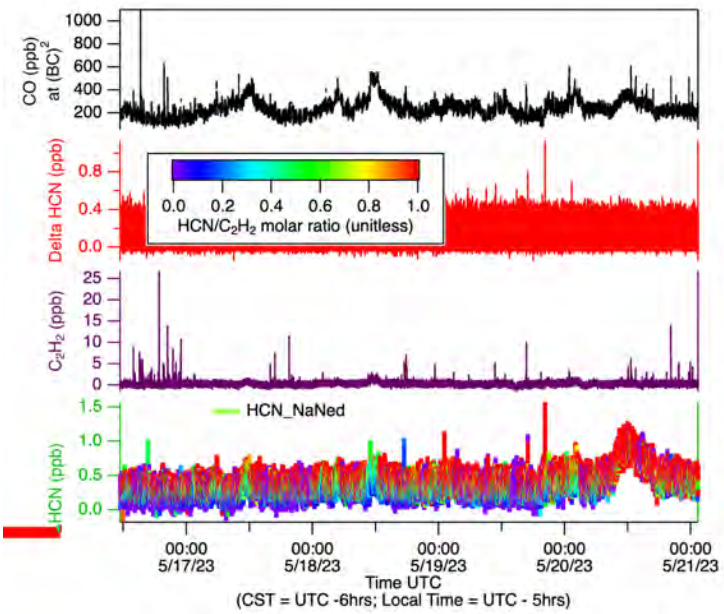

Figure 18. Time traces showing short- and long-duration HCN enhancements, colored by the HCN to C_2H_2 ratio.

In the graphs below, HCN data are plotted vs C_2H_2 for the entire time period. We include data just for spikes (left) and for the entire dataset (right). We see that HCN measurements above about 3 ppb consistently have C_2H_2 present (purple/blue dots); however, there are a significant number of spikes (red) that do not.

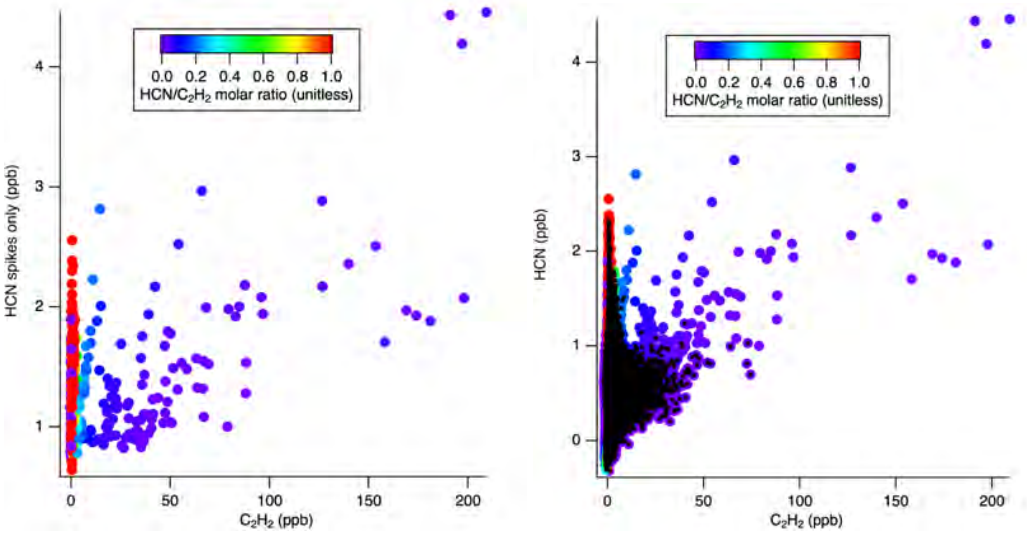

Figure 19. Scatter plots of HCN vs C_2H_2. The left plot shows only spike data, colored by HCN/C_2H_2 ratio. The left plot shows all measurement data, with data that is not considered a spike overlaid as black points.

CO was the traffic species used in prior campaign traffic explorations. Figure 20 data was taken by the Aerodyne Mobile Laboratory during the 2018 FIREX campaign. It shows a

strong background of biomass burning HCN (up to 4 ppb), with short spikes due to on-road traffic. The HCN/CO ratio in BB emissions is significantly higher than from traffic.

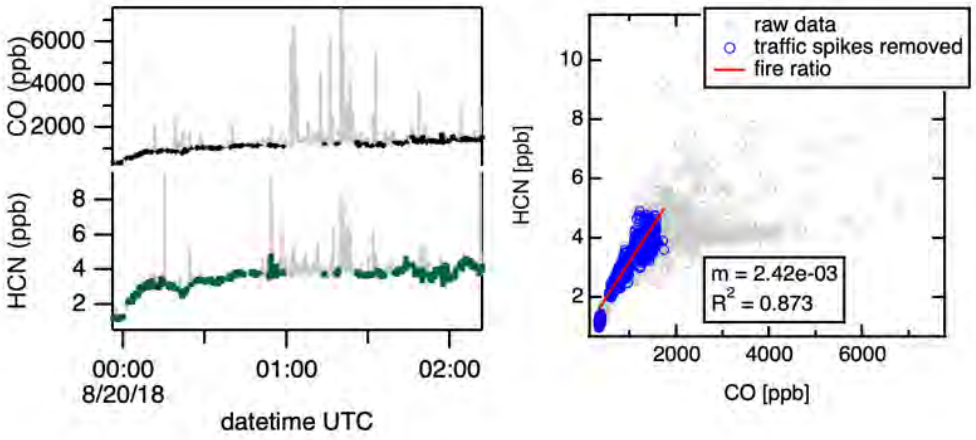

Figure 20. HCN and CO measurements during the 2018 FIREX campaign showing smoke-impacted enhancements along with spikes from traffic.

CO is not measured directly by the TILDAS instrument at the Fort Worth Northwest site. CO is available only at certain times (see Figure 10), and the time resolution is typically slower than for HCN. Acetylene is a secondary traffic tracer that can measured by the TILDAS instrument itself. This species may have advantages over CO in a traffic filtering procedure since its time response, data frequency, data coverage, and inlet lag will be identical to HCN.

Representative emission factors for hydrogen cyanide from biomass burning range between 0.29 – 1.52 g/kg Fuel [*Akagi et al.*, 2011] depending on fuel type, with considerable variability. Emission factors for HCN from vehicles are significantly lower, ranging between 0.003 – 0.15 g/kg Fuel, with diesel and biodiesel emitting less HCN than gasoline vehicles[*Moussa et al.*, 2016]. Moussa et al. measured 3 vehicles on dynamometers; follow-on studies of fleet-averaged emissions in real-world driving conditions noted significantly lower emission factors, 0.000 32 – 0.000 88 g HCN/kg fuel (interquartile range) [*Wren et al.*, 2018], calling into question these early results.

In this project, we are interested in the molar ratio of the enhancement in HCN to CO in a given plume, often termed the normalized excess mixing ratio (NEMR), or simply the emission ratio, ER, when the denominator is CO. ER for BB emissions range between 0.43 to 12.8 pptv ppb^{-1} [*Le Breton et al.*, 2013] ER for vehicle exhaust are not directly reported in the literature, but gasoline and diesel are more carbon-dense than wood/biomass. Tabulated data by Moussa *et al.* [2016] can be used to estimate molar ratios of HCN/CO in their study of 2.4 ± 2.3 mol HCN/mol CO, though these measurements have been called into question by Wren *et al*., who report an order of magnitude lower *emission factors* [*Wren et al.*, 2018]. Neither CO emission factors nor HCN/CO ratios were reported by Wren *et al*. We conclude that traffic HCN/CO should be

significantly lower than for biomass burning, but no reliable range of HCN/CO traffic ratios has yet been published, and the range likely overlaps with BB HCN/CO ratios on the lower end.

An example HCN:CO ER for a short-duration spike is shown below, with an ER_{HCN} of 0.19 pptv ppb^{-1}, lower than the expected range for BB plumes.

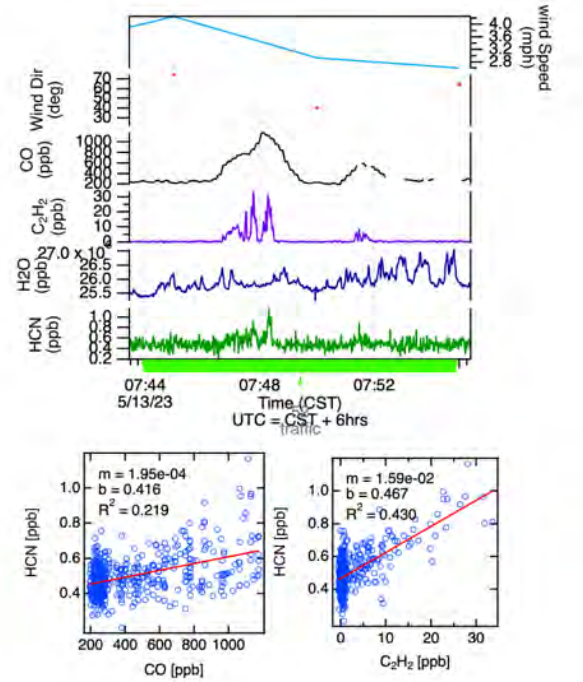

Figure 21. Example short-duration traffic plume and associated HCN/CO ratio.

In some instances, poor correlation between HCN and CO make the slope method of determining HCN:CO unreliable. In these cases, we can use the area under the plumes to determine the HCN:CO ratio, with the caveat that the choice of plume baseline becomes much more important. An example for one of the biomass burning plumes described in the following section is shown below. The slope method yields an HCN:CO ratio of 0.59 ppt ppb^{-1}, whereas the area method yields 1.1 ppt ppb^{-1}

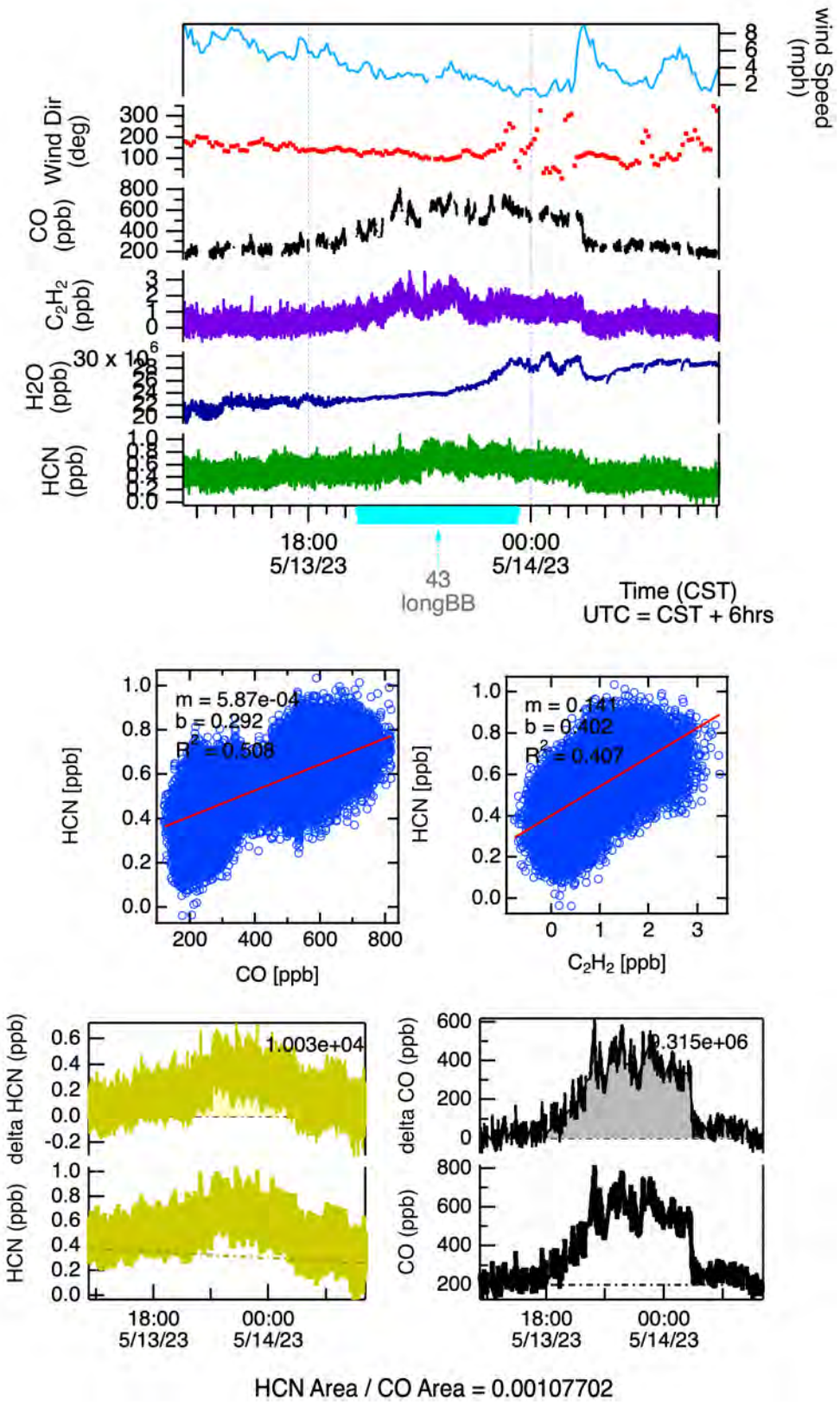

Figure 22. Time traces (top), correlation plots (middle, blue) and area-under-the-curve plots (bottom) for a biomass burning plume.

3.3 Comparison of HCN stationary measurement with mobile lab data

As part of AQRP 22-010, a secondary HCN instrument was deployed aboard the Aerodyne Mobile Laboratory (AML). Numerous additional instruments including speciated VOCs and Particulate matter were also on board. The AML was stationed at the Fort Worth Northwest site, with daily excursions off-site to measure point sources. Here, we compare only data when collocated with the $(BC)^2$ trailer.

Figure 3 plots HCN from the AML (project AQRP 22-010) against this project's HCN measurement (AQRP 22-060). The noise on the AML's HCN measurement was significantly enhanced (<300 ppt), which leads to the poor correlation and blur of data points shown below. We also note that the AML data is uncalibrated, but will be calibrated in time for the final reports.

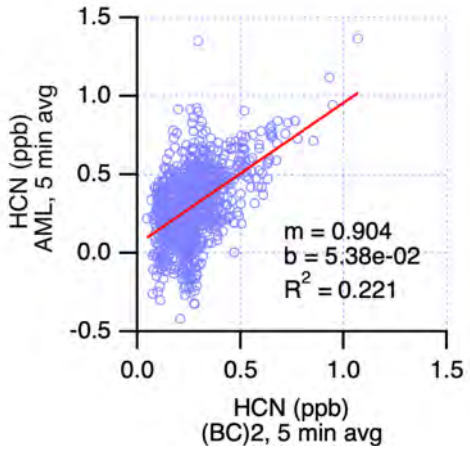

Figure 23. Comparison of uncalibrated AML HCN data to calibrated HCN data from the $(BC)^2$ trailer

The comparison between the two HCN measurements is more favorable during HCN enhancements, as shown below, where both HCN instruments measure an enhancement lasting 30 minutes. Other auxiliary tracers like carbon monoxide, organic particulate matter and AAE also show enhancements. The wind was from the southwest at this time.

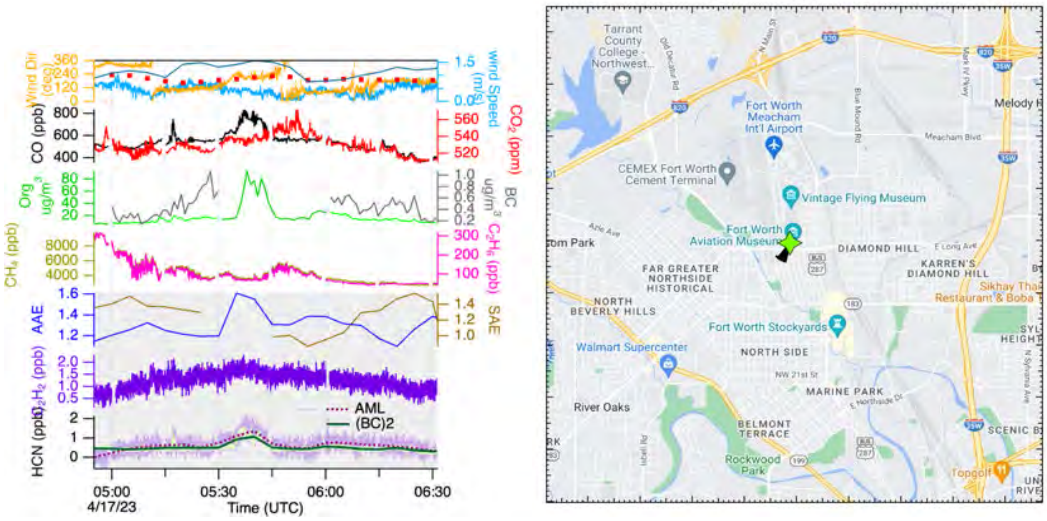

Figure 24. Time series (left) showing a potential biomass burning plume between 05:30 and 06:00 UTC. Enhancements in several BB tracers are observed, including HCN (measurements aboard the AML, green, and inside the $(BC)^2$ trailer, purple), AAE, Organic PM and CO. Shaded traces are from the $(BC)^2$ trailer unless otherwise noted. TCEQ-measured wind (5 min data) is shown alongside AML-measured wind (1s data). A map (right) showing the location of the Fort Worth Northwest site (green star) with wind barbs (black) indicating a wind from the southwest. CST = UTC -6h

3.3.1 Enhanced Biomass Burning Plume Identification

The first step of fire plume identification was to integrate the HCN dataset with the aerosol dataset. These are two very different biomass burning indicators: gas phase tracer and particle-phase optical properties. To add another dimension to the BB event identification, we also considered the absorption coefficient[1]. By considering the absorption coefficient, we are including a proxy for the magnitude of the BB event; in other words, we are assuming that as the absorption coefficient increases, the plume is more concentrated and the impact of the BB plume on local air quality is higher, for time periods where the AAE exceeds the BB threshold.

3.3.2 Case study 1: Multiple Biomass Burning Events

For the first case study we are considering the first week of April. In this period we have five Long BB events and multiple Short BB events (see Figure 25). We notice here that during the first Long BB event (4/7/2023 5:05), the AAE is enhanced, but the HCN remains low. During this early event, the absorption coefficient also remains low (average of 7.21 Mm^{-1}). For the third event (4/8/2023 18:15), the average absorption coefficient is much higher at 36 Mm^{-1} and the HCN peaks during this time as well. Although the peaks do not always exactly align, including the absorption coefficient improves understanding of the differences in the BB event types. The aerosol optical properties appear to be much more sensitive and can identify BB plumes even when

[1] The absorption coefficient will increase when there is a greater concentration of absorbing particles at the site (the absorption pathlength divided by the mass absorption coefficient will return the equivalent black carbon).

they are dilute. Only plumes that are more concentrated, with regards to the aerosol absorption coefficient, register as peaks in the HCN. This pattern can be seen in the four weeks included in Figure 27 as well, which indicates a consistency in this trend. To confirm this dependency, we correlated HCN against absorption coefficient for long and short duration events identified by the AAE > threshold (1.27; average AAE + one standard deviation) in Figure 28. There is a weak correlation; events with high HCN and high absorption coefficients should be investigated further for urban air quality impacts. There was no correlation between HCN and absorption for the very short/ local plumes.

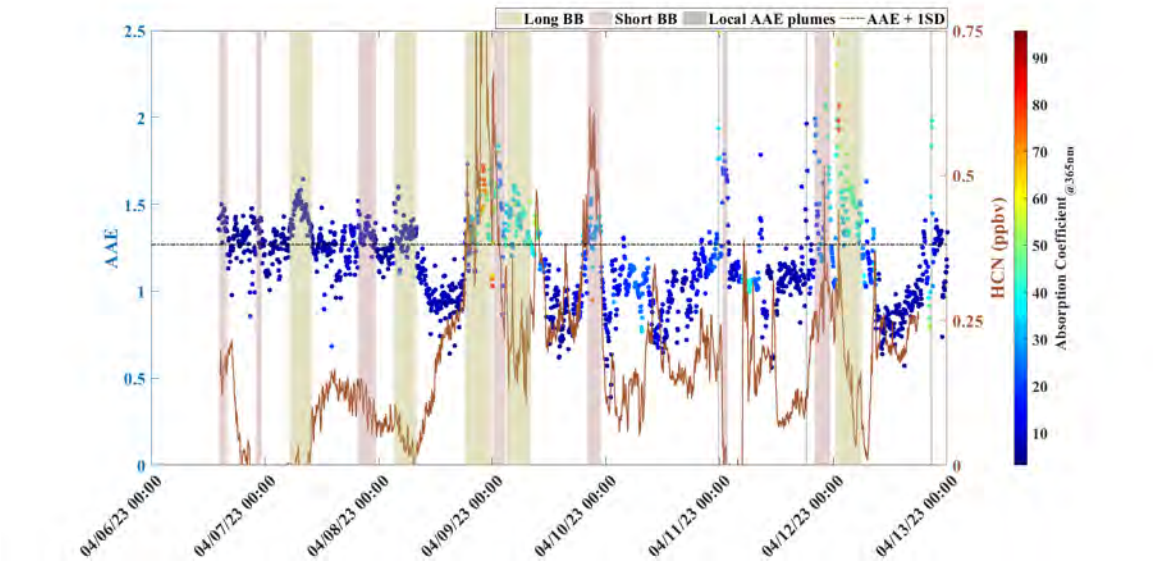

Figure 25. Time series (CST) of AAE colored with a gradient of absorption coefficient and HCN for the Fort Worth Site (April 6 – 13, 2023). BB events are highlighted based on AAE classification and duration.

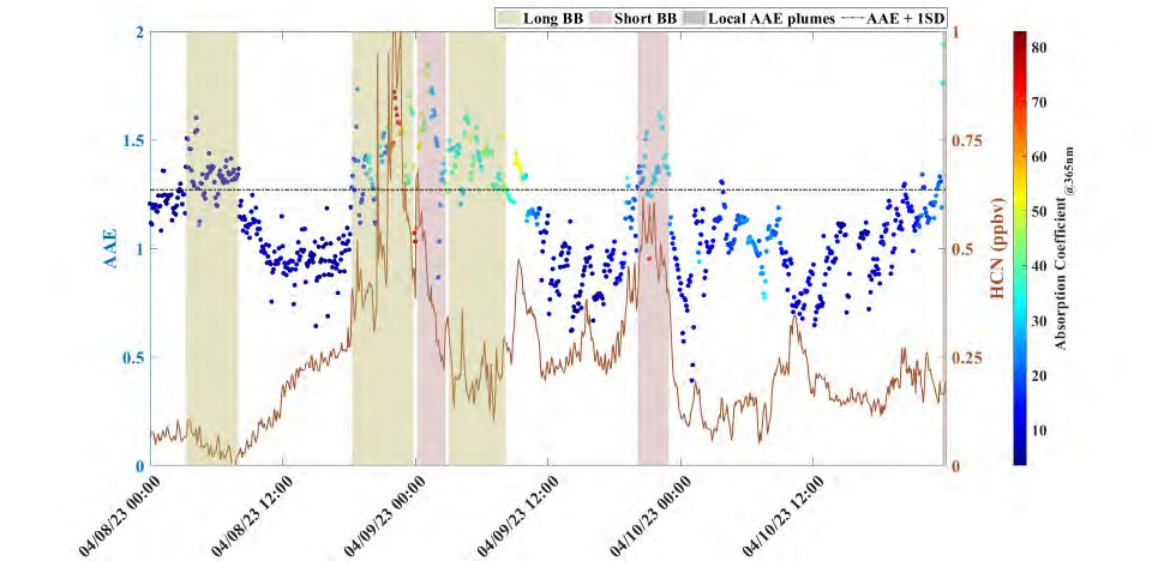

Figure 26. Focus on the Apr 7 – Apr 10 biomass burning event periods on the AAE and HCN time series (CST) for Fort Worth. BB events are highlighted based on AAE classification and duration.

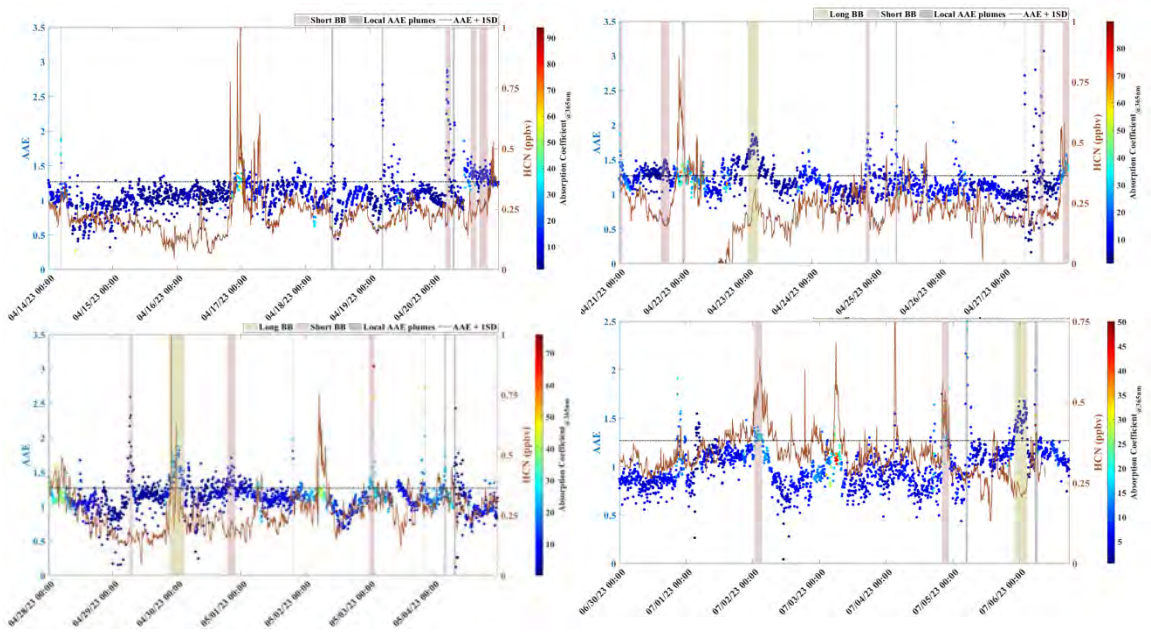

Figure 27 Time series (CST) of four different weeks series of AAE colored with a gradient of absorption coefficient and HCN for the Fort Worth Site (start dates: Apr 14, Apr 21, Apr 28 and Jun 30). The BB events are highlighted on each time periods. This time periods highlight the impact of the magnitude of the absorption coefficient on whether the BB event identified by AAE also has a peak in the HCN.

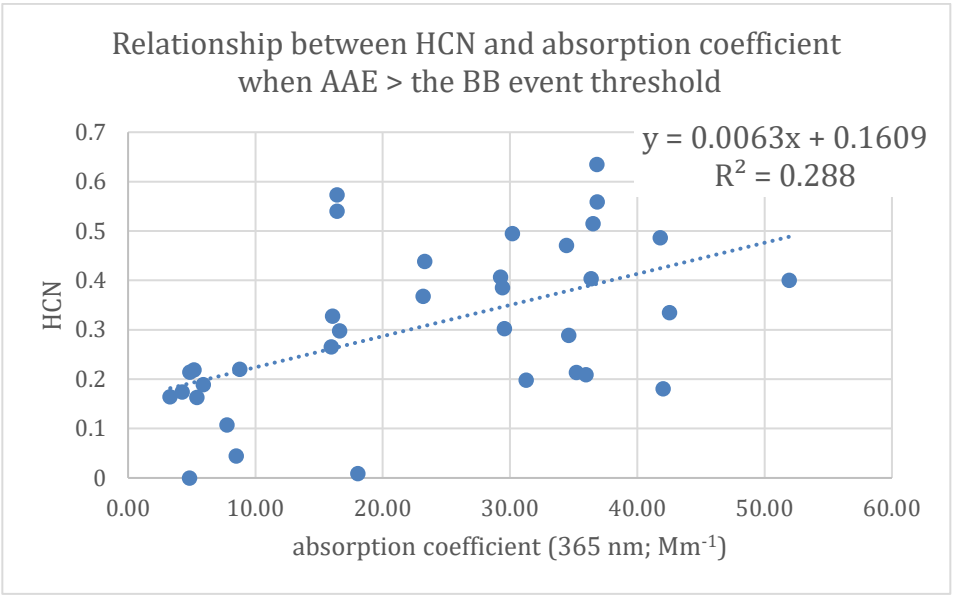

Figure 28. Correlation plot of average HCN vs absorption coefficient for long and short biomass burning (BB) events.

Examining additional tracers available from the HCN monitor, the $(BC)^2$ network site, the TCEQ CAMS site, and the Dallas Field Study project (Aerodyne Mobile Laboratory measurements via AQRP 22-010) provides further confirmation of these biomass burning events. In Figure 29, we plot HCN, C_2H_2, AAE and SAE (all from the $(BC)^2$ network trailer), but also include a number of tracers from the Aerodyne Mobile

Laboratory, which was co-located with the Fort Worth Northwest during the grey highlighted periods. AML measurements of the fire tracers acetonitrile (via Vocus Proton-Transfer-Reaction Mass-Spectrometer), elemental black carbon particulate matter and organic particulate matter (via Soot-Particle Aerosol Mass Spectrometer, SP-AMS) are correlated to the HCN and AAE traces.

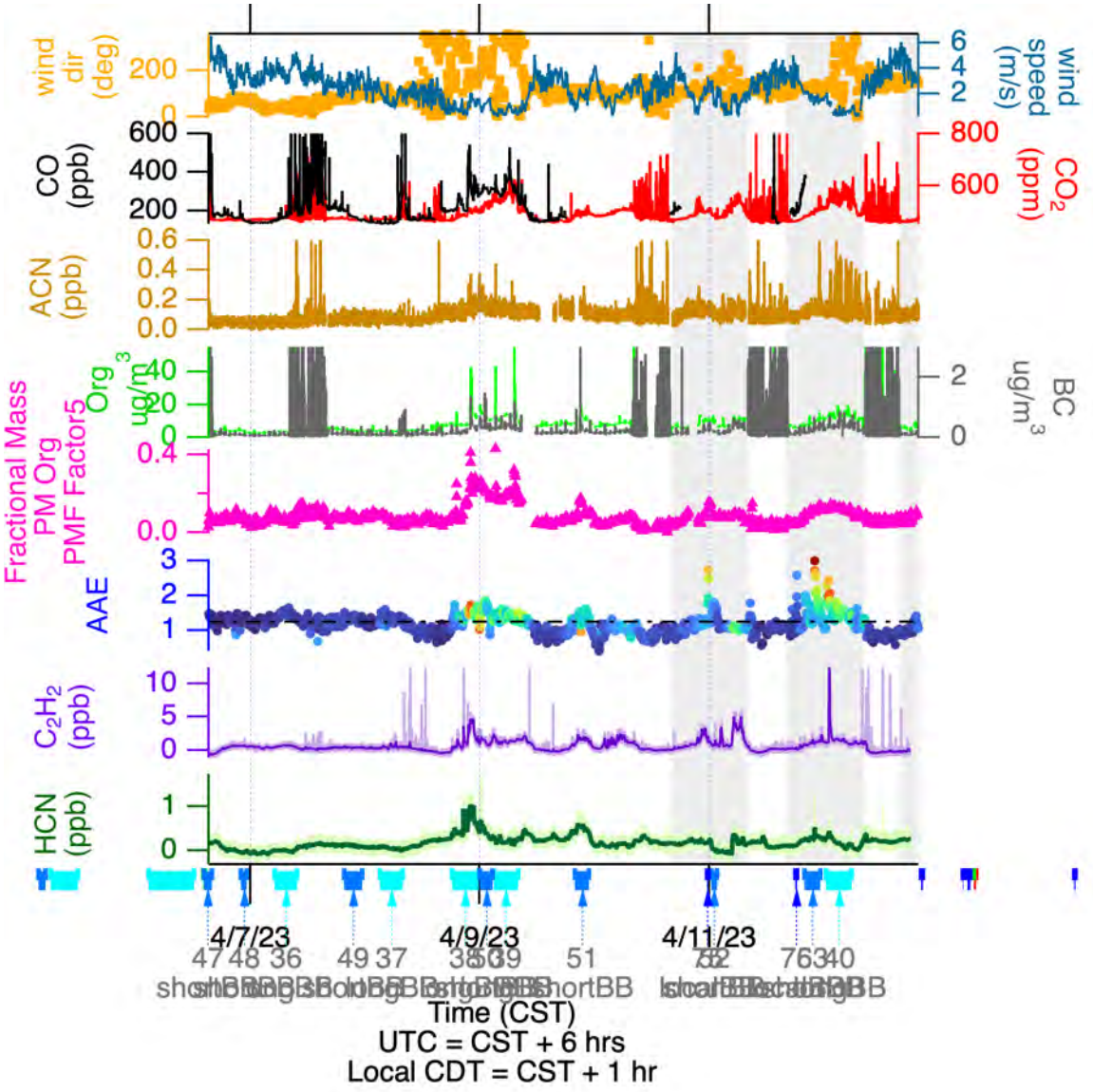

Figure 29. Time traces showing how numerous fire tracers agree, including AAE (colored by absorption, see scale in Figure 25), HCN, acetonitrile (ACN) and the biomass burning factor from a positive matrix factorization analysis of the SP-AMS-measured organic aerosol PMorg (pink).

Also shown is a time trace for the biomass burning factor derived from a Positive Matrix Factorization (PMF) analysis of the particulate matter organics mass spectra for the Dallas Field Study. PMF is a multivariate factor analysis technique developed by Paatero et al. [*Paatero*, 1997; *Paatero and Tapper*, 1994] to solve the bilinear factor model $x_{ij} = \Sigma_p g_{ip} f_{pj} + e_{ij}$ where x_{ij} are the measured values of j species in i samples, P are factors

comprised of constant source profiles (f_j, mass spectral data) with varying contributions over the time period of the dataset (g_i, time series), without any a priori assumptions of either mass spectral or time profile [*Lanz et al.*, 2007; *Ulbrich et al.*, 2009].

This PMF analysis has identified a group of organic particulate matter masses that vary together and have the signature of biomass burning. Details of the PMorg PMF analysis are available in the final report of AQRP Project 22-010 (PI: Fortner). A previous Texas study has shown good agreement between AMS and AAE-derived biomass burning event identification [*Shrestha et al.*, 2023].

Interestingly, the BB event with the highest-concentration HCN enhancement on right around midnight CST on 4/9/2023 is also observed in these tracers and the BB PMF factor, even though the Mobile Laboratory was located nearly 24 miles to the south-east, in Mansfield TX, at the Texan RV Ranch (Figure 30). This is further indication that this BB event was from long-range transport and affected a large swath of the Dallas-Fort-Worth metropolitan area.

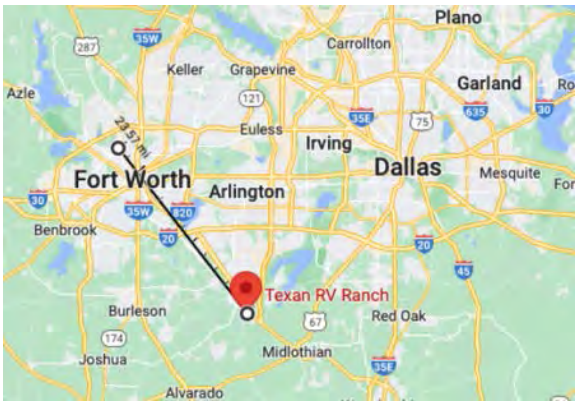

Figure 30. Texan RV Ranch (red pin marker) is 24 miles to the south-east of the Fort-Worth Northwest Site (circle marker)

3.3.3 Case study 2: Peaks in HCN without associated peaks in the AAE

In this next case study we evaluate peaks in HCN that do not share a BB signal with the AAE. In Figure 31 we see a strong peak in HCN and an AAE around 1, which also includes an increase in the absorption coefficient (May 12). Here it can be hypothesized that the increase in HCN may be related to traffic, which has an AAE near 1 and would include emissions of black carbon, which would increase the absorption coefficient. A second peak in HCN on May 13 does include an enhancement in AAE and in absorption coefficient, which indicates influence of biomass burning.

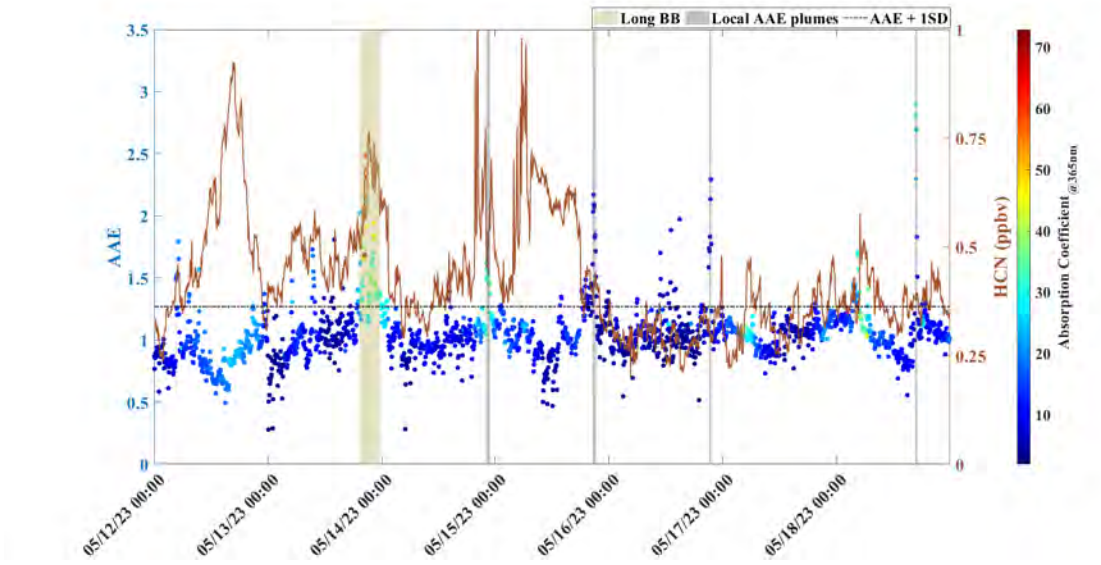

Figure 31. Time series (CST) of AAE colored with a gradient of absorption coefficient and HCN for the Fort Worth Site (May 12 – 18, 2023). BB events are highlighted based on AAE classification and duration.

Wind was from the SSE (155 - 175 deg) during the two main HCN peaks hypothesized to be of traffic origin, with HCN concentrations decreasing when winds changed to a northerly direction.

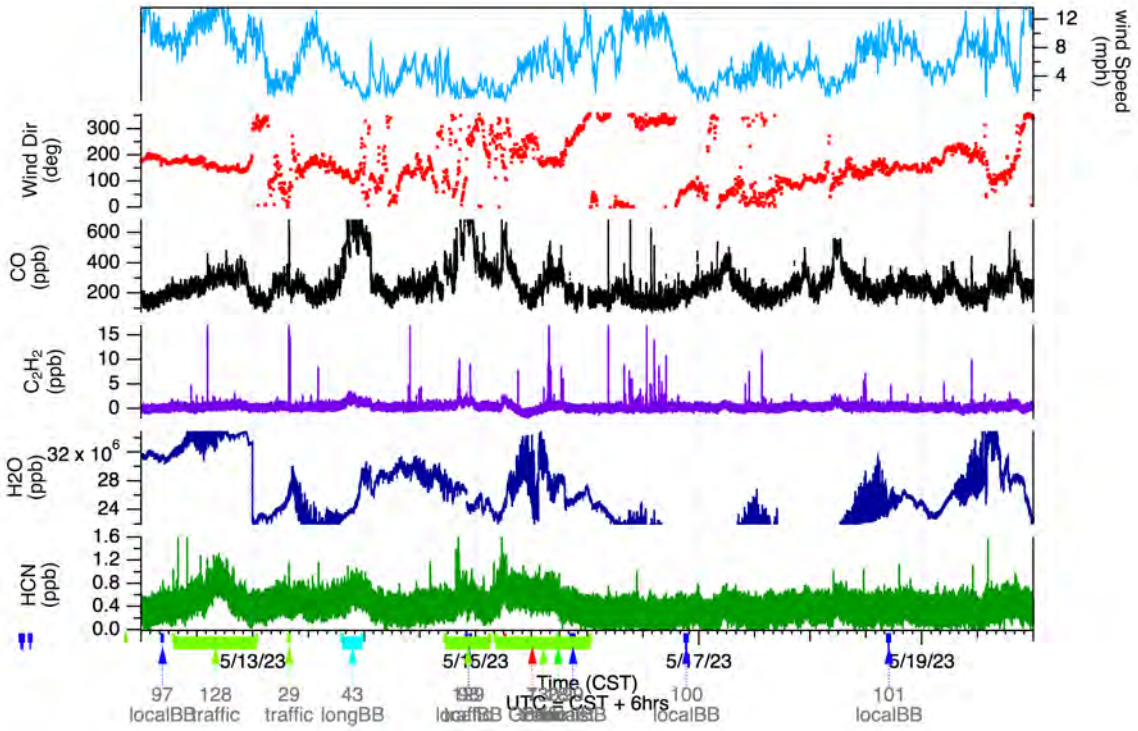

Figure 32. Case Study 2 time series showing other gas phase tracers like CO.

HCN is poorly correlated with CO during the HCN events not associated with AAE enhancements (Figure 32), with HCN:CO emission ratios of 0.8 – 2 ppt/ppb (area method, range for the three plumes). As an example, the first HCN-only plume is shown in Figure 33, and the CO:HCN ratio calculated via both slope and area. Interestingly, the plume that is flagged as long range BB using the optical parameters has a HCN:CO of 1 ppt ppb^{-1} (area method), within the same range as the other HCN-only plumes. Recall that expected BB ERs range between 0.43 to 12.8 ppt ppb^{-1} [*Le Breton et al.*, 2013] Thus, the HCN:CO ratio for all these plumes would be consistent with biomass burning. However, due to the poor correlation between HCN and CO, it is likely that the sampled airmass included traffic influence, at least in the CO.

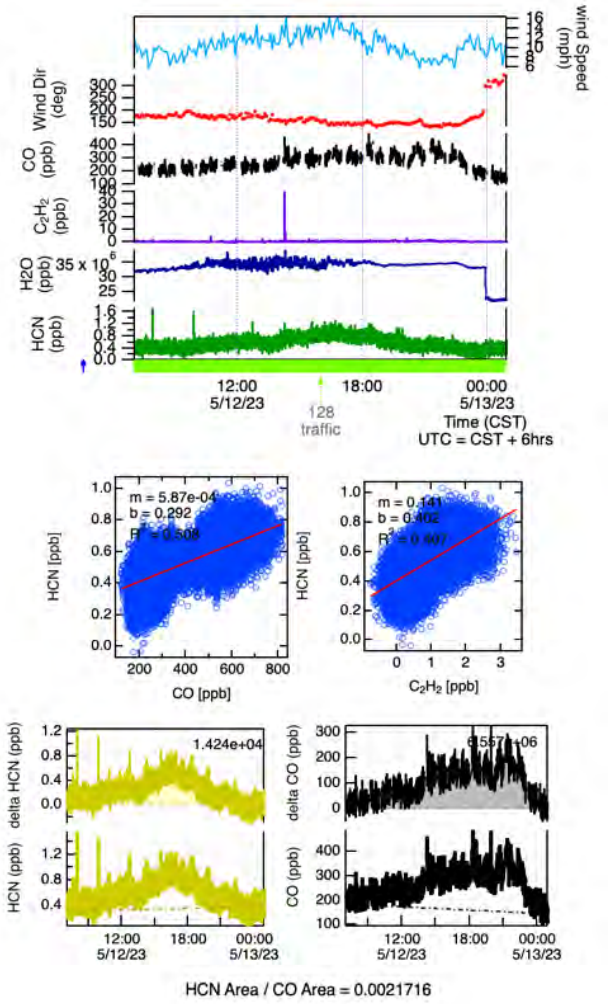

Figure 33. HCN/CO ratios calculated for the first HCN plume of Case Study 2.

This divergence between the long-lived gas tracers and the aerosol tracer may also indicate processing of the plume during transport, e.g. precipitation, which would remove aerosol more efficiently than long-lived gas species like CO. Both CO and HCN have comparable atmospheric lifetimes (~2 months for CO; 5 months for HCN). The primary loss mechanism for CO is via atmospheric oxidation with OH radical; in contrast,

HCN loss is dominated by aqueous-phase uptake [*Bruno et al.*, 2023]. Though water is important for HCN uptake, the process is slow.

3.3.4 Case Study 3. Peaks in HCN that do not share a peak in AAE, with Enhanced Tracers.

Biomass burning is readily distinguishable in the PMF of the particulate matter organics measured by SP-AMS. The BB factor has a characteristic ion at $C_2H_4O_2^+$, corresponding to a fragment of levoglucosan, a hydrocarbon produced in fires. The PMF results from the AMS-measured organic aerosol provide excellent detectivity of biomass burning events, but this type of analysis relies on an expensive instrument, with expensive (computationally, time, training) analysis.

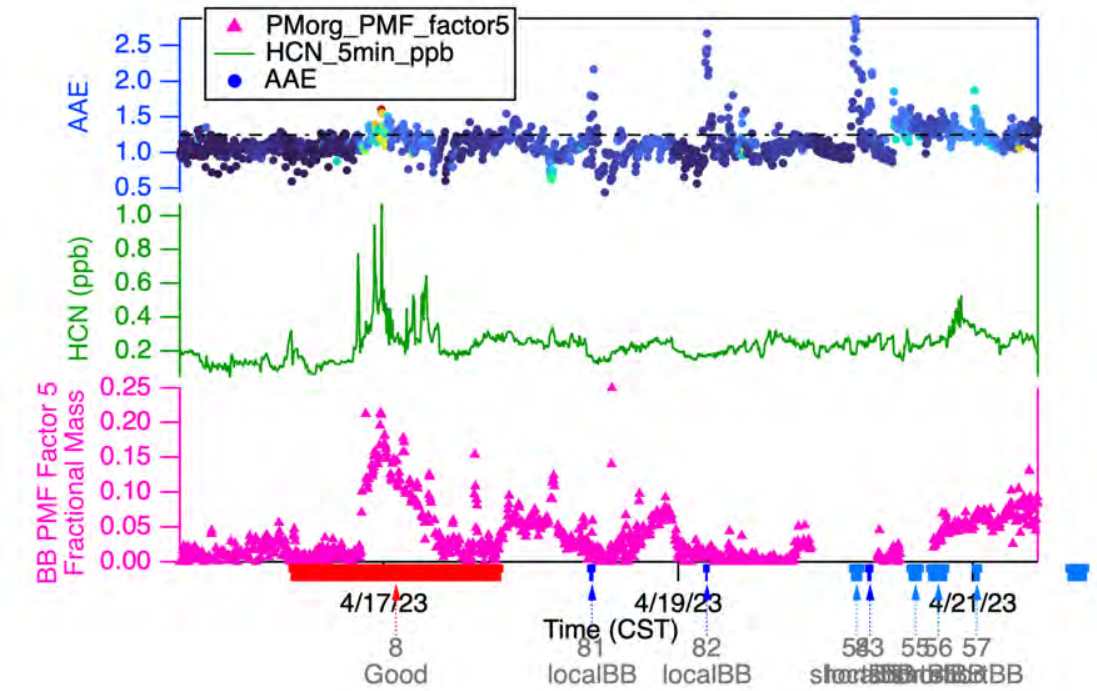

Figure 34. Time series of AAE (colored by absorption, see scale in Fig), HCN and the biomass burning factor from a PMF analysis of SP-AMS-measured organic aerosol.

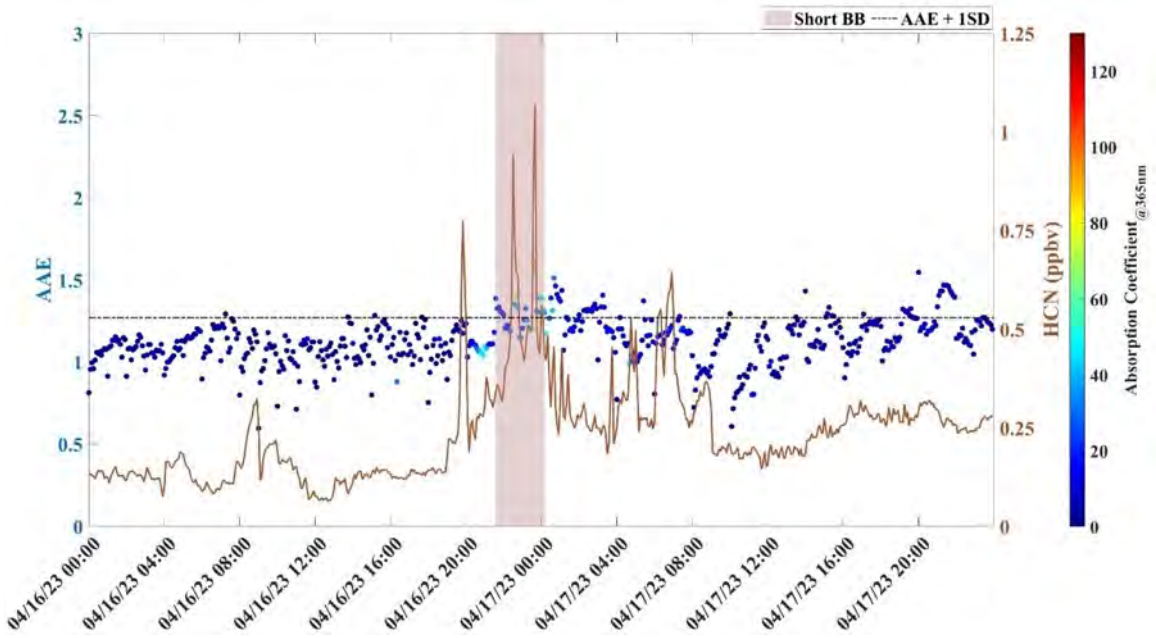

Figure 35. Time series of AAE (colored by absorption) and HCN highlighting the BB plume.

In Figure 34, we see an HCN plume (underlined in red) along with a spike in the absorption coefficient (at 365 nm). The PMF BB factor also peaks at this time, confirming the presence of biomass burning aerosol. We also see that although the PMF BB factor shows a clear peak, the magnitude of this peak is only 20% of the total organic aerosol mass, meaning that 80% of the organic aerosol mass has other sources. The AAE is above threshold but not as enhanced as some other events (AAE of 1.30, with a campaign threshold of 1.27), however the absorption coefficient is also higher at this time (average of 36.5 Mm^{-1}). In this case, HCN is serving as a BB tracer with signal-to-noise analogous to the PMF results, and this even in the presence of a mixed smoke and urban aerosol plume.

3.3.5 Case Study 4. Elevated AAE, with low SAE and low HCN

A dust event is clearly depicted impacting the site just before noon on 4/20. This enhances the AAE, depresses the SAE and causes a large peak in the scattering coefficient. There is a small peak in the HCN which is not reflected in the AAE, perhaps due to the on-going influence of the dust plume. The AAE remains elevated, but the absorption coefficients are very low, indicating a non-consequential BB influence. This combination of instruments allows a complex view of the changing sources during this time and the relative air quality impacts.

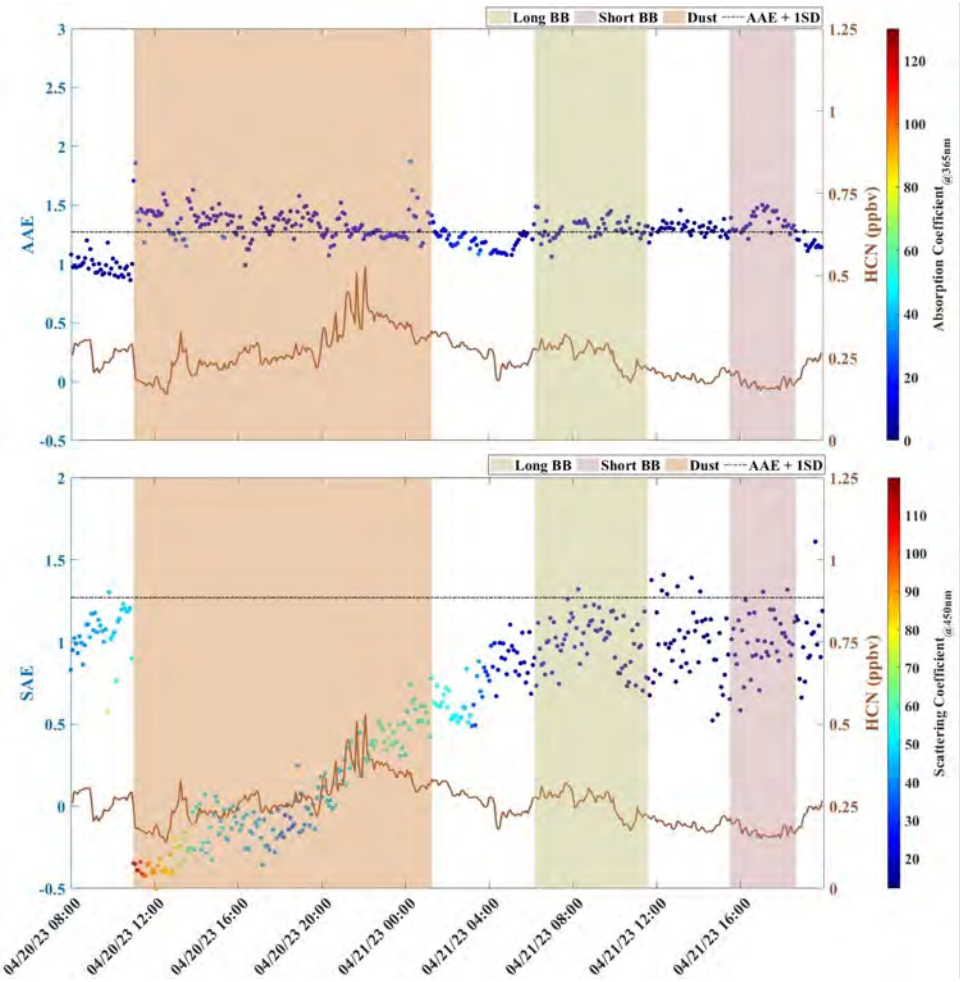

Figure 36 Top figure plots AAE, absorption coefficient and HCN, while bottom figure includes SAE, scattering coefficient and HCN.

4.0 Conclusions

HCN was successfully measured at TCEQ's "Fort Worth Northwest" site from April 6th, 2023 to July 6th, 2023. The dataset includes 83 measurement days (gaps when the instrument was down are not counted), exceeding the 66-day goal. The instrument performed to specifications, with a few gaps and periods of missing zeroes, requiring quality assurance. We maintained a strong collaboration between this project (AQRP 22-060, PI: Yacovitch, Co-PIs: Sheesley, Usenko) and two related projects measuring at this same site: the $(BC)^2$ network expansion project (2021 campaign final report for TCEQ PGA: 582-21-22317-016); and the mobile laboratory measurements stationed at this site at night (PI: Ed Fortner, Aerodyne Research, AQRP 22-010).

HCN data quality assurance and analysis has been completed, focusing on filtering out of short-duration spikes due to nearby traffic. Ratios of HCN to C_2H_2 were investigated, and short-duration spikes were found to have a significant range of ratios.

BB events have been identified (Appendix B) and explored through a series of case studies. The first week in April is one such case study, showing several BB events of long and short duration.

We have identified several short-duration spikes with HCN:CO ratios indicative of traffic. However, we do not conclusively identify any broad/regional traffic-only HCN plumes. Certain broad HCN-only plumes without associated enhancements in AAE were investigated (times not overlapping Dallas Field Study), and HCN/CO ratios for these plumes fall within the range of expected values for BB plumes. The poor HCN/CO correlations suggest plumes of mixed origin, and back-trajectory investigations indicate that the airmasses transited regions of heavy rainfall, potentially washing out the aerosols.

During the 3-week Dallas Field Study (AQRP Project 22-010), the HCN measurement agrees with a positive matrix factorization analysis of the organic aerosol measured by the Soot Particle Aerosol Mass Spectrometer, and identifies at least one BB event that had an AAE enhancement just above the threshold, but with a strong enhancement in the absorption coefficient. The reason may be that this event consisted of an aerosol plume of mixed origin (biomass burning organic aerosol comprised 20% of the total organic aerosol mass). At other times, the absence of HCN suggests certain identified peaks are *not* of BB origin or have a very low aerosol absorption coefficient. HCN is shown to be a high sensitivity BB tracer even in this urban environment, yielding comparable BB plume detection as results from the PMF analysis of organic aerosol composition, but without the associated computational and analysis cost.

We observe that the absorption coefficient (a proxy for the total smoke loading) is elevated when enhancements in HCN are seen during BB events. Thus, including the co-located HCN measurement and the absorption coefficient in BB plume detection may make it easier to identify BB plumes that will have a more pronounced impact on local air quality. The HCN monitor provides a continuous, 1-second, sensitive metric of biomass burning, without the need for filters.

Combustion conditions during the wildfire and aging of the plume during transport can both impact the chemical composition and the optical properties of the smoke plume. The addition of the real time gas phase HCN tracer combined with AAE and absorption coefficients improved characterization of the magnitude of the plumes that impacted the Dallas-Fort Worth area in Apr – Jul, 2023.

5.0 Recommendations for Future Work

This pilot project to include HCN measurements in the (BC)2 network suggests several additional avenues for future work.

First, on the instrument side, **eliminating consumable zero gas, and improving HCN instrument recovery after power outages is warranted**. For this campaign, the use of ultra-zero air tanks for HCN zeroing was a proven and simple zeroing method to reduce instrument drift. However, the use of a scrubber or zero-air-generator to remove HCN from ambient air during zeroes is an alternate scheme, and would eliminate the need for tank changes (1 done during the campaign), and allow for easier long-term monitoring. The data gaps present in the HCN measurement were all a result of power outages at the site. Future deployments will benefit from improved and automated instrument recovery after power failures, which are inevitable in any long-term deployment.

Next, this study, as well as the related $(BC)^2$ network project and the Dallas Field Study conducted under AQRP 22-010 motivate continued and enhanced monitoring for biomass burning events in Texas. **Monitoring at multiple sites should continue and be expanded.** The fortuitous measurement of a biomass burning event by this project at the Fort-Worth-Northwest site, and by the AQRP 22-010 mobile laboratory when stationed further south in Mansfield indicated a clear regional biomass burning influence. The $(BC)^2$ network is a good example of utilizing multiple sites within a metropolitan area to improve identification of regional events. Additionally, **longer/continuous measurements should be done to encompass the increasing variability in when "fire season" occurs in Texas**. Trends in Texas wildfires in the past few years show a great deal of variability the number of fires/BB events detected month-to-month, as is borne out by $(BC)^2$ number of detected events by year (Figure 37). This project's measurements, spanning April – early July 2023, detected numerous BB events in the early spring, as expected. However, a period of drought after the end of the measurement period is also resulting in wildfires in the state during July-August, well into the summer. Finally, this study motivates **the addition of measurements of chemical composition** to biomass burning studies, to supplement optical properties currently in use. Additional measurements allowed for increased confidence in identifying smoke plumes during this project. HCN is a good candidate species, with detectivity comparable to sophisticated and expensive results obtained via particulate matter organic aerosol factorization.

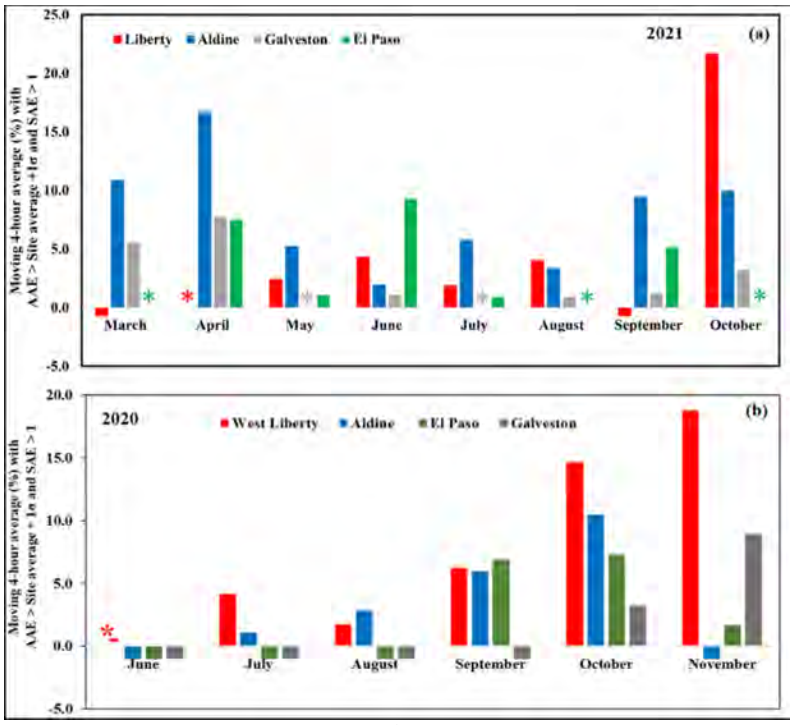

Figure 37. Number of detected BB events by the $(BC)^2$ network in 2020 and 2021.

Finally, additional work is warranted using the datasets collected as part of this study to **investigate the impacts of measured biomass burning plumes on ozone in Dallas Fort-Worth.** The 1-hour daily maximum ozone (ppb) in the Dallas Fort-Worth region (data from TCEQ) is shown in Figure 38 during the Dallas Field Study is shown below. Though no ozone exceedances were observed in this period, the highest recorded peak occurred on 4/17, coincident with one of our case studies finding biomass burning influence in the region.

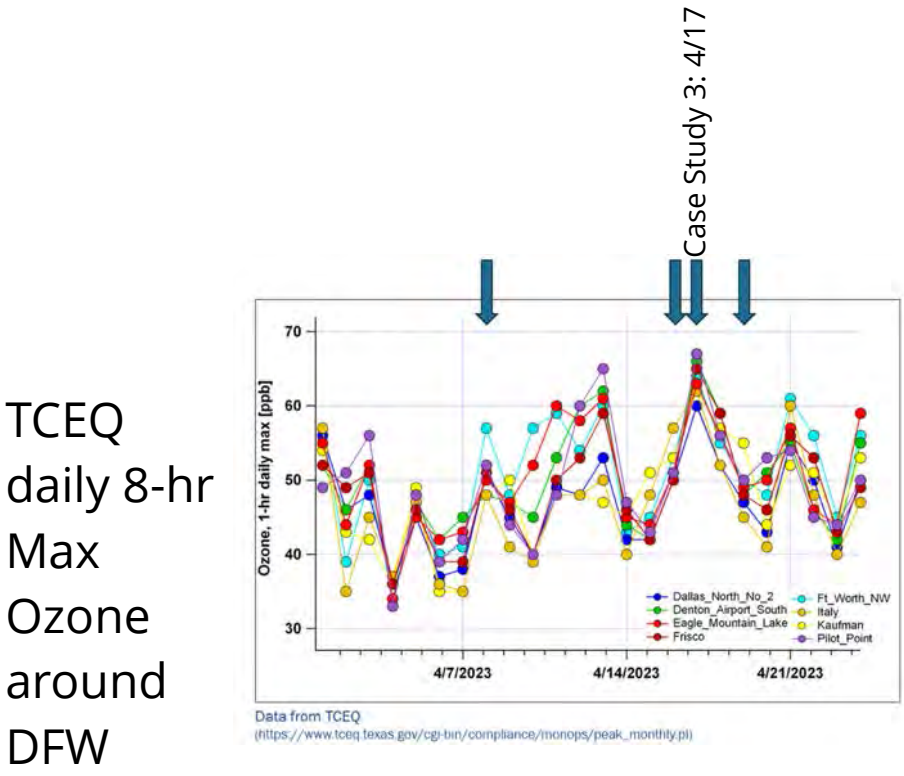

Figure 38. Peak 1-hr daily ozone in the Dallas Fort Worth area.

6.0 References

Abatzoglou, J. T., and A. P. Williams (2016), Impact of anthropogenic climate change on wildfire across western US forests, *Proc. Nat. Acad. Sci.*, *113*(42), 11770-11775, doi:doi:10.1073/pnas.1607171113.

Akagi, S. K., R. J. Yokelson, C. Wiedinmyer, M. J. Alvarado, J. S. Reid, T. Karl, J. D. Crounse, and P. O. Wennberg (2011), Emission factors for open and domestic biomass burning for use in atmospheric models, *Atmos. Chem. Phys.*, *11*(9), 4039-4072, doi:10.5194/acp-11-4039-2011.

Bergstrom, R. W., P. Pilewskie, P. B. Russell, J. Redemann, T. C. Bond, P. K. Quinn, and B. Sierau (2007), Spectral absorption properties of atmospheric aerosols, *Atmos. Chem. Phys.*, *7*(23), 5937-5943, doi:10.5194/acp-7-5937-2007.

Bruno, A. G., J. J. Harrison, M. P. Chipperfield, D. P. Moore, R. J. Pope, C. Wilson, E. Mahieu, and J. Notholt (2023), Atmospheric distribution of HCN from satellite observations and 3-D model simulations, *Atmos. Chem. Phys.*, *23*(8), 4849-4861, doi:10.5194/acp-23-4849-2023.

GAW (2011), Global Atmosphere Watch (GAW) Report No. 200: WMO/GAW Standard Operating Procedures for In-Situ Measurements of Aerosol Mass Concentration,

Light Scattering and Light Absorption., *Rep.*, World Meteorological Organization. https://library.wmo.int/doc_num.php?explnum_id=7166

Gordon, I. E., L. S. Rothman, C. Hill, R. V. Kochanov, Y. Tan, P. F. Bernath, M. Birk, V. Boudon, A. Campargue, K. V. Chance, B. J. Drouin, J. M. Flaud, R. R. Gamache, J. T. Hodges, D. Jacquemart, V. I. Perevalov, A. Perrin, K. P. Shine, M. A. H. Smith, J. Tennyson, G. C. Toon, H. Tran, V. G. Tyuterev, A. Barbe, A. G. Császár, V. M. Devi, T. Furtenbacher, J. J. Harrison, J. M. Hartmann, A. Jolly, T. J. Johnson, T. Karman, I. Kleiner, A. A. Kyuberis, J. Loos, O. M. Lyulin, S. T. Massie, S. N. Mikhailenko, N. Moazzen-Ahmadi, H. S. P. Müller, O. V. Naumenko, A. V. Nikitin, O. L. Polyansky, M. Rey, M. Rotger, S. W. Sharpe, K. Sung, E. Starikova, S. A. Tashkun, J. V. Auwera, G. Wagner, J. Wilzewski, P. Wcisło, S. Yu, and E. J. Zak (2017), The HITRAN2016 molecular spectroscopic database, *Journal of Quantitative Spectroscopy and Radiative Transfer*, *203*, 3-69, doi:https://doi.org/10.1016/j.jqsrt.2017.06.038.

Hayden, K., S. M. Li, J. Liggio, M. Wheeler, J. Wentzell, A. Leithead, P. Brickell, R. Mittermeier, Z. Oldham, C. Mihele, R. Staebler, S. Moussa, A. Darlington, A. Steffen, M. Wolde, D. Thompson, J. Chen, D. Griffin, E. Eckert, J. Ditto, M. He, and D. Gentner (2022), Reconciling the total carbon budget for boreal forest wildfire emissions using airborne observations, *Atmos. Chem. Phys. Discuss.*, *2022*, 1-62, doi:10.5194/acp-2022-245.

Jaffe, D. A., N. Wigder, N. Downey, G. Pfister, A. Boynard, and S. B. Reid (2013), Impact of Wildfires on Ozone Exceptional Events in the Western U.S., *Environ. Sci. Technol.*, *47*(19), 11065-11072, doi:10.1021/es402164f.

Kirchstetter, T. W., T. Novakov, and P. V. Hobbs (2004), Evidence that the spectral dependence of light absorption by aerosols is affected by organic carbon, *J. Geophys. Res., [Atmos.]*, *109*(D21), doi:https://doi.org/10.1029/2004JD004999.

Lanz, V. A., M. R. Alfarra, U. Baltensperger, B. Buchmann, C. Hueglin, and A. S. H. Prévôt (2007), Source apportionment of submicron organic aerosols at an urban site by factor analytical modelling of aerosol mass spectra, *Atmos. Chem. Phys.*, *7*(6), 1503-1522.

Le Breton, M., A. Bacak, J. B. A. Muller, S. J. O'Shea, P. Xiao, M. N. R. Ashfold, M. C. Cooke, R. Batt, D. E. Shallcross, D. E. Oram, G. Forster, S. J. B. Bauguitte, P. I. Palmer, M. Parrington, A. C. Lewis, J. D. Lee, and C. J. Percival (2013), Airborne hydrogen cyanide measurements using a chemical ionisation mass spectrometer for the plume identification of biomass burning forest fires, *Atmos. Chem. Phys.*, *13*(18), 9217-9232, doi:10.5194/acp-13-9217-2013.

Liu, X., L. G. Huey, R. J. Yokelson, V. Selimovic, I. J. Simpson, M. Müller, J. L. Jimenez, P. Campuzano-Jost, A. J. Beyersdorf, D. R. Blake, Z. Butterfield, Y. Choi, J. D. Crounse, D. A. Day, G. S. Diskin, M. K. Dubey, E. Fortner, T. F. Hanisco, W. Hu, L. E. King, L. Kleinman, S. Meinardi, T. Mikoviny, T. B. Onasch, B. B. Palm, J. Peischl, I. B. Pollack, T. B. Ryerson, G. W. Sachse, A. J. Sedlacek, J. E. Shilling, S. Springston, J. M. St. Clair, D. J. Tanner, A. P. Teng, P. O. Wennberg, A. Wisthaler, and G. M. Wolfe (2017), Airborne measurements of western U.S. wildfire emissions: Comparison with prescribed burning and air quality implications, *J.*

Geophys. Res., [Atmos.], *122*(11), 6108-6129, doi:https://doi.org/10.1002/2016JD026315.

McManus, J. B., M. S. Zahniser, D. D. Nelson, J. H. Shorter, S. C. Herndon, D. Jervis, M. Agnese, R. McGovern, T. I. Yacovitch, and J. R. Roscioli (2015), Recent progress in laser-based trace gas instruments: performance and noise analysis, *Applied Physics B*, *119*(1), 203-218, doi:10.1007/s00340-015-6033-0.

Moosmüller, H., and R. K. Chakrabarty (2011), Technical Note: Simple analytical relationships between Ångström coefficients of aerosol extinction, scattering, absorption, and single scattering albedo, *Atmos. Chem. Phys.*, *11*(20), 10677-10680, doi:10.5194/acp-11-10677-2011.

Moussa, S. G., A. Leithead, S.-M. Li, T. W. Chan, J. J. B. Wentzell, C. Stroud, J. Zhang, P. Lee, G. Lu, J. R. Brook, K. Hayden, J. Narayan, and J. Liggio (2016), Emissions of hydrogen cyanide from on-road gasoline and diesel vehicles, *Atmos. Environ.*, *131*, 185-195, doi:https://doi.org/10.1016/j.atmosenv.2016.01.050.

Müller, T., J. S. Henzing, G. de Leeuw, A. Wiedensohler, A. Alastuey, H. Angelov, M. Bizjak, M. Collaud Coen, J. E. Engström, C. Gruening, R. Hillamo, A. Hoffer, K. Imre, P. Ivanow, G. Jennings, J. Y. Sun, N. Kalivitis, H. Karlsson, M. Komppula, P. Laj, S. M. Li, C. Lunder, A. Marinoni, S. Martins dos Santos, M. Moerman, A. Nowak, J. A. Ogren, A. Petzold, J. M. Pichon, S. Rodriquez, S. Sharma, P. J. Sheridan, K. Teinilä, T. Tuch, M. Viana, A. Virkkula, E. Weingartner, R. Wilhelm, and Y. Q. Wang (2011), Characterization and intercomparison of aerosol absorption photometers: result of two intercomparison workshops, *Atmos. Meas. Tech.*, *4*(2), 245-268, doi:10.5194/amt-4-245-2011.

Nielsen-Gammon, J., S. Holman, A. Buley, S. Jorgensen, J. Escobedo, C. Ott, J. Dedrick, and A. Van Fleet (2021), Assessment of Historic and Future Trends of Extreme Weather In Texas, 1900-2036 (2021 Update), *Rep.*, 42 pp, Texas A&M University. https://climatexas.tamu.edu/products/texas-extreme-weather-report/index.html

Ogren, J. A. (2010), Comment on “Calibration and Intercomparison of Filter-Based Measurements of Visible Light Absorption by Aerosols”, *Aerosol Sci. Tech.*, *44*(8), 589-591, doi:10.1080/02786826.2010.482111.

Ogren, J. A., J. Wendell, E. Andrews, and P. J. Sheridan (2017), Continuous light absorption photometer for long-term studies, *Atmos. Meas. Tech.*, *10*(12), 4805-4818, doi:10.5194/amt-10-4805-2017.

Paatero, P. (1997), A weighted non-negative least squares algorithm for three-way 'PARAFAC' factor analysis, *Chemometrics Intell. Lab. Syst.*, *38*(2), 223-242.

Paatero, P., and U. Tapper (1994), Positive Matrix Factorization - a Nonnegative Factor Model with Optimal Utilization of Error-Estimates of Data Values, *Environmetrics*, *5*(2), 111-126.

Schmeisser, L., E. Andrews, J. A. Ogren, P. Sheridan, A. Jefferson, S. Sharma, J. E. Kim, J. P. Sherman, M. Sorribas, I. Kalapov, T. Arsov, C. Angelov, O. L. Mayol-Bracero, C. Labuschagne, S. W. Kim, A. Hoffer, N. H. Lin, H. P. Chia, M. Bergin, J. Sun, P. Liu, and H. Wu (2017), Classifying aerosol type using in situ surface spectral aerosol

optical properties, *Atmos. Chem. Phys.*, *17*(19), 12097-12120, doi:10.5194/acp-17-12097-2017.

Schnaiter, M., M. Gimmler, I. Llamas, C. Linke, C. Jäger, and H. Mutschke (2006), Strong spectral dependence of light absorption by organic carbon particles formed by propane combustion, *Atmos. Chem. Phys.*, *6*(10), 2981-2990, doi:10.5194/acp-6-2981-2006.

Schnaiter, M., C. Linke, O. Möhler, K.-H. Naumann, H. Saathoff, R. Wagner, U. Schurath, and B. Wehner (2005), Absorption amplification of black carbon internally mixed with secondary organic aerosol, *J. Geophys. Res., [Atmos.]*, *110*(D19), doi:https://doi.org/10.1029/2005JD006046.

Selimovic, V., R. J. Yokelson, G. R. McMeeking, and S. Coefield (2020), Aerosol Mass and Optical Properties, Smoke Influence on O3, and High NO3 Production Rates in a Western U.S. City Impacted by Wildfires, *J. Geophys. Res., [Atmos.]*, *125*(16), e2020JD032791, doi:https://doi.org/10.1029/2020JD032791.

Shrestha, S., S. Zhou, M. Mehra, M. C. Guagenti, S. Yoon, S. L. Alvarez, F. Guo, C. Y. Chao, J. H. Flynn Iii, Y. Wang, R. J. Griffin, S. Usenko, and R. J. Sheesley (2023), Evaluation of aerosol- and gas-phase tracers for identification of transported biomass burning emissions in an industrially influenced location in Texas, USA, *EGUsphere*, *2023*, 1-33, doi:10.5194/egusphere-2023-367.

Ulbrich, I. M., M. R. Canagaratna, Q. Zhang, D. R. Worsnop, and J. L. Jimenez (2009), Interpretation of organic components from Positive Matrix Factorization of aerosol mass spectrometric data, *Atmos. Chem. Phys.*, *9*(9), 2891-2918.

Warneke, C., J. P. Schwarz, J. Dibb, O. Kalashnikova, G. Frost, J. Al-Saad, S. S. Brown, W. A. Brewer, A. Soja, F. C. Seidel, R. A. Washenfelder, E. B. Wiggins, R. H. Moore, B. E. Anderson, C. Jordan, T. I. Yacovitch, S. C. Herndon, S. Liu, T. Kuwayama, D. Jaffe, N. Johnston, V. Selimovic, R. Yokelson, D. M. Giles, B. N. Holben, P. Goloub, I. Popovici, M. Trainer, A. Kumar, R. B. Pierce, D. Fahey, J. Roberts, E. M. Gargulinski, D. A. Peterson, X. Ye, L. H. Thapa, P. E. Saide, C. H. Fite, C. D. Holmes, S. Wang, M. M. Coggon, Z. C. J. Decker, C. E. Stockwell, L. Xu, G. Gkatzelis, K. Aikin, B. Lefer, J. Kaspari, D. Griffin, L. Zeng, R. Weber, M. Hastings, J. Chai, G. M. Wolfe, T. F. Hanisco, J. Liao, P. Campuzano Jost, H. Guo, J. L. Jimenez, J. Crawford, and T. F.-A. S. Team (2023), Fire Influence on Regional to Global Environments and Air Quality (FIREX-AQ), *J. Geophys. Res., [Atmos.]*, *128*(2), e2022JD037758, doi:https://doi.org/10.1029/2022JD037758.

Westerling, A. L., H. G. Hidalgo, D. R. Cayan, and T. W. Swetnam (2006), Warming and Earlier Spring Increase Western U.S. Forest Wildfire Activity, *Science*, *313*(5789), 940-943, doi:doi:10.1126/science.1128834.

Wren, S. N., J. Liggio, Y. Han, K. Hayden, G. Lu, C. M. Mihele, R. L. Mittermeier, C. Stroud, J. J. B. Wentzell, and J. R. Brook (2018), Elucidating real-world vehicle emission factors from mobile measurements over a large metropolitan region: a focus on isocyanic acid, hydrogen cyanide, and black carbon, *Atmos. Chem. Phys.*, *18*(23), 16979-17001, doi:10.5194/acp-18-16979-2018.

Appendix A. Quality Assurance Document for HCN dataset.

This quality assurance document describes the quality control and quality assurance steps taken to produce the 1-second HCN measurement dataset.

HCN measurements at the Fort Worth Northwest site (GPS coordinates of 32.8058182, -97.3565229) were conducted in spring/summer 2023. The campaign spanned 4/6/23 20:31 UTC to 7/6/23 13:58 UTC. This includes 83 measurement days (not counting gaps). A summary HCN time series is shown below, with fast 1-second data (green) and 5-minute average data (black) is shown below.

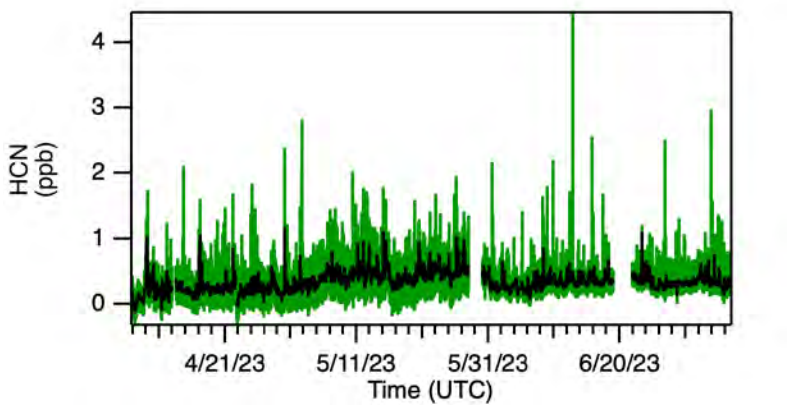

Figure 39. Overview of HCN measurements performed at the Fort Worth Northwest site.

Two HCN data products are produced: the 1-second measurement data, and the 5-minute average data. Both datasets include a readme file, in addition to this QA document. The file names include the year, month, and date of the data revision (*yyyymmdd*).

- HCNatBC2_ARIdata_*yyyymmdd*.txt
- HCNatBC2_ARIdata_Readme_*yyyymmdd*.txt
- HCNatBC2_5min_ARIdata_*yyyymmdd*.txt
- HCNatBC2_5min_ARIdata_Readme_*yyyymmdd*.txt

The 1-second dataset includes spike-filtered data. Time is reported in UTC time, and a secondary time trace is included for the CST time zone (inactive time zone, 1 hr off from local time), since CST is used in the $(BC)^2$ network species.

The 5-minute averages were produced to aid comparison to the slower stationary site measurements. These data include the time stamp, which is the mid-time for the 5-minute period. They also include the start time of the measurement, for consistency with other $(BC)^2$ reported species.

Species Measured

- Hydrogen cyanide (HCN), ambient air mixing ratio, ppb, calibrated

- Acetylene (C_2H_2), ambient air mixing ratio, ppb, uncalibrated
- Water (H_2O), ambient air mixing ratio, ppb, uncalibrated

HCN was measured in the spectral region shown in Figure 40. Other species present in the spectrum include water (strong absorber around 3286.2 cm^{-1}) and acetylene (dual peaks in blue). CO_2 is included in the fit (tiny red shoulders to HCN) but does not have enough absorption strength to show enhancements during the magnitude of biomass burning or traffic plume observed during this campaign. For this reason, CO_2 data from this instrument is not reported.

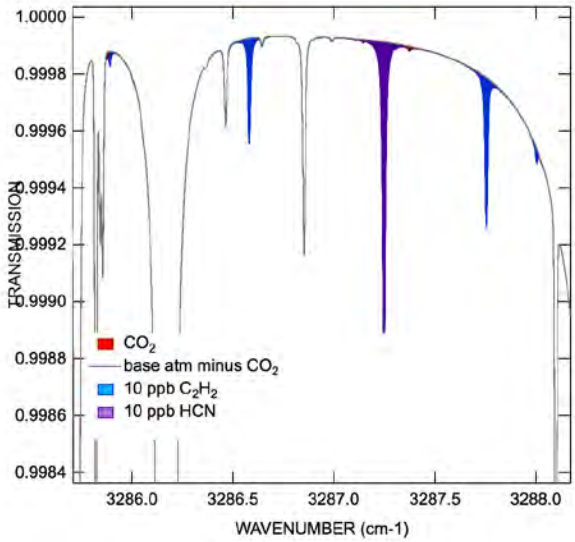

Figure 40. Spectral window for the TILDAS measurement of HCN (purple). Acetylene (C_2H_2, blue) and water are also present in this spectral region.

Offsets

There were a handful of periods during the campaign where the HCN instrument collected data with no autobackground gas flowing. Usually, the spectral ratioing was turned off as well, so as not to collect zero mixing ratio data by zeroing on ambient. When this is done, we collect raw HCN data that has a persistent positive offset. An example is shown below. For this time period, we see that the positive offset gets corrected when the first successful autobackground is done at 4/13/23 14:00 UTC. The data prior to this zero is manually offset by -0.74, which matches the baselines around 14:00.

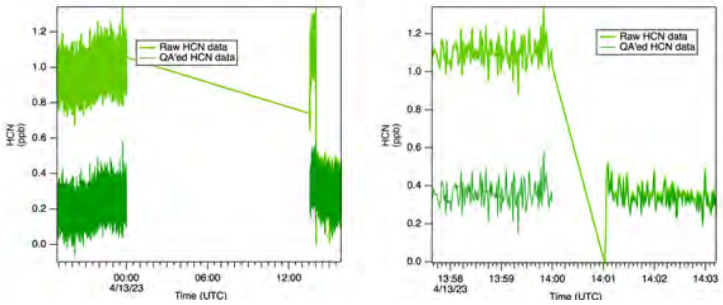

Figure 41. Time series (left) and zoom in (right) of a period requiring manual offset.

A record of all offsets applied is present in the QA code at the end of this section, with the command titled "QA_offsetCorrect". Start and stop times and offset magnitude (in ppb) are noted. For example, for the data above, this command was used to apply the offset of -0.74012935 ppb.

// offset times with no zero
QA_offsetCorrect(dataWave=root:a_HCN:HCN_NaNed, timeWave=root:a_HCN:str_source_rtime, startTime=3763657859.769150, stopTime=3764188798.879720, offset=-0.74012935) // 04/06/2023 20:30:59, 04/12/2023 23:59:58

The HCN spectrometer collects and saves archival spectra in addition to the computed mixing ratios. For this campaign, we collected several types of spectra: "BG" spectra, which are average backgrounds during UZA overblow; "SIG" spectra, which are divided by the background spectrum; and "RAW" spectra, which are undivided spectra. Saving both RAW and SIG data doubles the space requirements of the dataset, but gives more flexibility in cases when refits are needed.

At other times, refit data was used to help determine offsets. In the example below, autobackground-on-ambient data was collected prior to about 5/31/23 02:00 (mixing ratios around 0). Then, ABG was turned off, at which point unbackgrounded data was taken (mixing ratios elevated). The "RAW" spectral files were refit to span this entire period, which allows us to correctly offset the autobackground-on-ambient data.

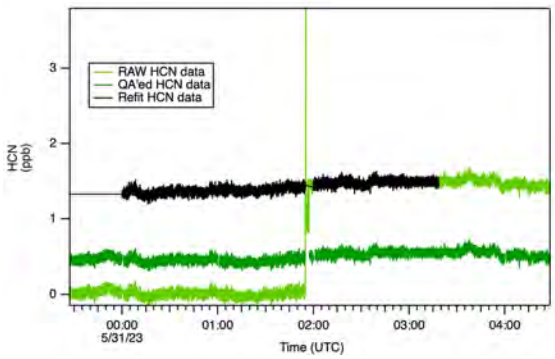

Figure 42. Data on 5/31 showing raw HCN (pale green), QA'ed HCN (deep green) and refit of "RAW" spectral files (black).

Calibration

Aerodyne scientists, present in Fort-Worth as part of the AQRP 22-010 mobile laboratory project, were able to conduct an HCN instrument calibration for this project on 4/22/2023. Results of HCN calibration are shown below:

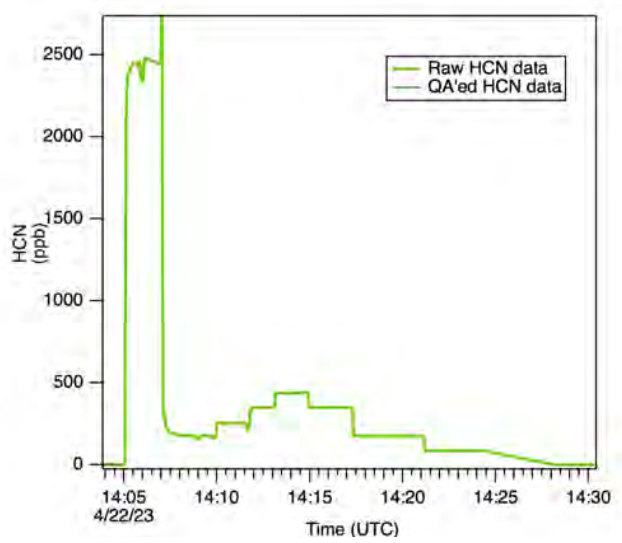

Figure 43. Time series for the calibration on 4/22/2023. The strong signal at 14:05 is prior to the start of the calibration. The sloped period at 14:25 is a data gap.

Table 1. Summary of calibration points for the 4/22 calibration

4/22/23	14 UTC	*5 ppm HCN in N_2 balance*	
HCN Calibration (Field Site)			
Small HCN flow (sccm)	*Big UZA flow (SLPM)*	*HCN Standard Conc (ppb)*	*HCN Measured Conc (ppb)*
500	5.65	406.504	437.615
400	5.65	330.579	350.197
200	5.65	170.940	174.056
100	5.65	86.957	86.36
0	5.65	0	0.0327
300	5.65	252.101	251.356

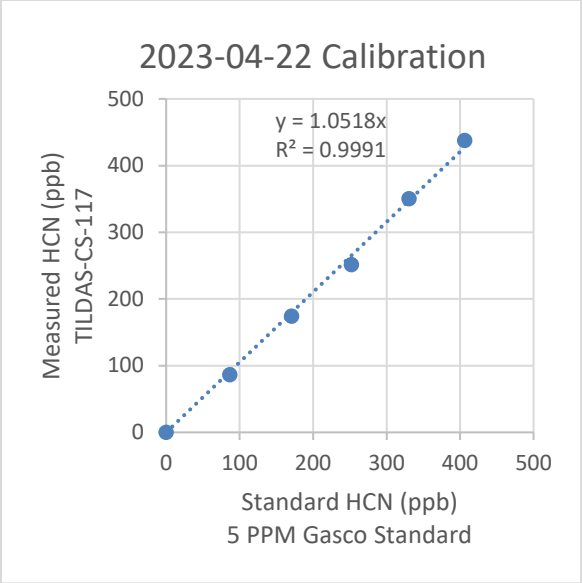

Figure 44. Calibration trace showing measured HCN versus delivered HCN.

A calibration factor *m* = 1.05 was determined on 4/22/2023, where HCN_meas = *m* * HCN_true. This means that raw HCN values will be divided by 1.05 in the final QA'ed dataset. The instrument was undergoing autobackgrounds, and had a cell pressure of 40 Torr during this measurement. This calibration uses a 5 ppm HCN GasCo standard purchased from Concept Controls (Quotation 11002165) in a balance of zero air.

Two other calibrations were attempted during this measurement campaign. The first, done on done on 10/26/2022 at Baylor campus, revealed a calibration factor of 0.795. (Initial workup of this calibration, reported in monthly reports, plotted data incorrectly with a slope of *m*=1.26) We will discard this first calibration factor since the instrument was sent back to Aerodyne for repair and assessment prior to the above campaign calibration.

A second calibration was attempted on the day of de-installation. This calibration displayed significant lag in reaching their setpoints (Figure 45). The calibration also used an over-sized 5 SLPM Alicat flow meter to deliver 100 sccm and lower concentrations. For this reason, we discard this calibration as well.

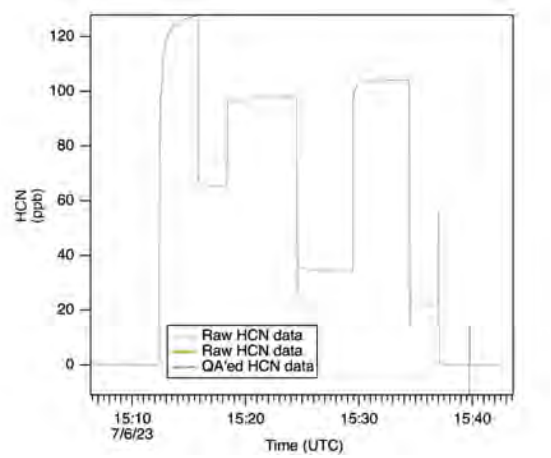

Figure 45. Calibration data on 7/6/2023 showing a slow time constant.

We summarize the three calibrations performed in the table below. Our calibration factor chosen is 1.052.

Table 2. Record of HCN calibrations.

Date	HCN cal factor	Note
10/22/22	0.795*	After detector failure, and before instrument shipped back
4/22/23	1.052	During DFW Campaign: Matt
7/8/23	1.483*	Before de-installation: Sascha. Oversized Alicat for small flow

* Discarded. See above.

Full QA code

The code below is written in Wavemetric's Igor Pro scripting language. It uses some proprietary analysis functions to automate various QA steps. This consists of a full record of the QA steps taken.

```
Setdatafolder root:a_HCN
duplicate/o root:a_HCNreload:str_source_rtime, source_rtime, str_source_rtime
duplicate/o root:a_HCNreload:HCN, HCN
duplicate/o root:a_HCNreload:C2H2_Fix, C2H2
duplicate/o root:a_HCNreload:H2O, H2O
// but use Field 4 water when present.
H2O = numtype(root:a_HCNreload:H2O_Field4[p]) != 2 ?
root:a_HCNreload:H2O_Field4[p]:H2O[p]
AML_DataFolderBased_SAKN("root:a_HCN", text2datetime("4/6/23 20:30:59"),
text2datetime("7/6/23 13:58:55"))

  QAQCw_ResetAllWaves()

// QA blacklist
  QAQCw_NanThisClass("Blacklist;cal")
```

// some of thsi data may be recoverable
QAQCw_NanThisClass("needsQA")

QAQCw_NanThisClass("needsQA", tokenList="H2O;C2H2")

QAQCw_NaNlargeDataGaps("HCN",3.000000)
QAQCw_NaNlargeDataGaps("C2H2",3.000000)
QAQCw_NaNlargeDataGaps("H2O",3.000000)

// offset times with no zero
QA_offsetCorrect(dataWave=root:a_HCN:HCN_NaNed, timeWave=root:a_HCN:str_source_rtime, startTime=3763657859.769150, stopTime=3764188798.879720, offset=-0.74012935) // 04/06/2023 20:30:59, 04/12/2023 23:59:58

QA_offsetCorrect(dataWave=root:a_HCN:HCN_NaNed, timeWave=root:a_HCN:str_source_rtime, startTime=3765054229.754350, stopTime=3765056399.232690, offset=-0.65259209) // 04/23/2023 00:23:49, 04/23/2023 00:59:59

// Big period with no zeroes in June
QA_offsetCorrect(dataWave=root:a_HCN:HCN_NaNed, timeWave=root:a_HCN:str_source_rtime, startTime=3768342895.164520, stopTime=text2datetime("6/8/23 18:00:05"), offset=-0.914) // 05/31/2023 01:54:55, 6/8/23 17:59:59

// zeroes turned off. matched to refit.
QA_offsetCorrect(dataWave=root:a_HCN:HCN_NaNed, timeWave=root:a_HCN:str_source_rtime, startTime=3766996462.733730, stopTime=3767040000.314790, offset=-0.378182) // 05/15/2023 11:54:22, 05/16/2023 00:00:00

// no zeroes, but ABG on
QA_offsetCorrect(dataWave=root:a_HCN:HCN_NaNed, timeWave=root:a_HCN:str_source_rtime, startTime=3768253261.167190, stopTime=3768342895.164520, offset=0.469) // 05/30/2023 01:01:01, 05/31/2023 01:54:55

// brief period of ABG off within above time.
QA_offsetCorrect(dataWave=root:a_HCN:HCN_NaNed, timeWave=root:a_HCN:str_source_rtime, startTime=3768319923.621050, stopTime=3768321599.695110, offset=-1.2813641) // 05/30/2023 19:32:03, 05/30/2023 19:59:59

QA_offsetCorrect(dataWave=root:a_HCN:HCN_NaNed, timeWave=root:a_HCN:str_source_rtime, startTime=3764237640.127740, stopTime=3764239199.601460, offset=-0.72359324) // 04/13/2023 13:34:00, 04/13/2023 13:59:59

QAQCw_zeroWaveReset(); QAQCw_zeroDefine("HCN",4,"00:00:00",3600,60)
QAQCw_NaNZeroes(0,0,tokens="HCN;C2H2")
QAQCw_NaNZeroes(0,60,tokens="H2O")

/////// Calibration

root:a_HCN:HCN_NaNed/= 1.0518

// sharp spikes
setdatafolder root:a_HCN
QAQCw_FiveMinMinimum(root:a_HCN:str_source_rtime, root:a_HCN:HCN_NaNed, avgTime=10) // 10 second plumes
duplicate/o HCN_NaNed_5minmin deltaHCN
duplicate/o HCN_NaNed HCN_noSpikes
deltaHCN = HCN_NaNed - HCN_NaNed_5minMin

HCN_noSpikes = deltaHCN[p] > 0.6 ? NaN : HCN_NoSpikes[p]
// could do something like this if not same time
// QAQCw_clipIntensity("deltaHCN","CObkg",0,10,time2inletTF=0)

duplicate/o HCN_NaNed ratio
ratio = C2H2_Naned/HCN_Naned

// Data output, fast data
setdatafolder root:a_HCN
duplicate/o str_source_rtime, datetimeUTC
// there is a 55 second offset between the HCN monitor and the BB2 network CO measurement.
// The HCN monitor is fast.
// this is an empirical number taken from sharp CO spikes due to traffic, which often have C2H2 spikes associated with them.
// The HCN monitor time agrees with the AML time when at the site, so it is likely either a BB2 instrument inlet delay, or that coupled with a time server difference.
datetimeUTC = str_source_rtime + 55

duplicate/o str_source_rtime datetimeCST // inactive
*datetimeCST = datetimeUTC - 6 * 3600*

Appendix B. Biomass Burning Events

Tables 1-3 include the data associated with the identified Long, Short and Local BB events including the time period of the event, average values for Absorption Ångström Exponent (AAE), wind speed, wind direction, and absorption coefficient (σ_{abs}) by wavelength. The AAE threshold (average AAE plus one standard deviation) for the Fort Worth site during the AQRP HCN campaign was 1.27.

Table 1: Long BB event (> 4 hr)

Start	End	AAE Threshold	Average AAE	Max AAE	Min AAE	SAE	Smoke Overhead	BT through smoke	Absorption coefficient Red	Absorption coefficient Green	Absorption coefficient Blue	Average HCN (ppbv)
4/1/23 19:30	4/2/23 0:35	1.27	1.57	2.11	1.26	1.32	N	Y	17.79	22.83	42.61	NaN
4/5/23 6:15	4/5/23 12:00	1.27	1.67	2.90	0.75	1.04	N	Y	2.29	3.14	6.25	NaN
4/6/23 2:45	4/6/23 12:15	1.27	1.41	1.53	1.22	1.52	N	Y	4.09	5.24	8.95	NaN
4/7/23 5:05	4/7/23 9:55	1.27	1.45	1.65	1.30	1.56	N	Y	3.21	4.12	7.21	NaN
4/8/23 3:15	4/8/23 8:00	1.27	1.34	1.60	1.10	1.53	N	Y	4.06	5.12	8.50	0.04
4/8/23 18:15	4/8/23 23:50	1.27	1.42	1.73	1.11	1.57	N	Y	16.33	20.60	36.85	0.56
4/9/23 3:00	4/9/23 8:10	1.27	1.41	1.61	1.20	1.81	N	Y	16.44	20.70	35.98	0.21
4/12/23 0:35	4/12/23 6:00	1.27	1.57	2.43	1.26	1.43	Y	Y	17.25	23.05	42.03	0.18

4/23/23 0:05	4/23/23 4:05	1.27	1.67	1.87	1.23	1.65	N	Y	2.04	2.72	5.18	0.22
4/29/23 21:05	4/30/23 2:55	1.27	1.53	2.04	1.25	1.68	N	Y	6.75	8.71	16.07	0.33
5/13/23 19:20	5/13/23 23:40	1.27	1.55	2.49	1.14	1.47	Y	Y	15.22	19.95	36.84	0.63
5/30/23 21:05	5/31/23 1:50	1.27	1.42	2.20	1.00	1.61	Y	Y	13.04	17.09	29.43	0.39

Table 2: Short BB event (1-4 hr)

Start	End	AAE Threshold	Average AAE	Max AAE	Min AAE	SAE	Smoke Overhead	BT through smoke	Absorption coefficient Red	Absorption coefficient Green	Absorption coefficient Blue	Average HCN (ppbv)
4/6/23 14:20	4/6/23 16:00	1.27	1.41	1.50	1.28	1.52	N	Y	2.47	3.18	5.42	0.16
4/6/23 22:05	4/6/23 23:20	1.27	1.36	1.42	1.25	1.70	N	Y	2.27	2.90	4.82	NaN
4/7/23 19:40	4/7/23 23:25	1.27	1.34	1.52	1.20	1.53	N	Y	3.69	4.67	7.78	0.11
4/9/23 0:10	4/9/23 2:45	1.27	1.50	1.85	0.87	1.73	N	Y	15.74	19.95	36.38	0.40
4/9/23 20:05	4/9/23 22:55	1.27	1.36	1.61	0.95	1.91	N	Y	14.34	17.77	30.21	0.50
4/11/23 0:35	4/11/23 1:45	1.27	1.65	1.79	1.38	1.92	Y	Y	7.12	9.79	18.07	0.01
4/11/23 20:05	4/11/23 23:25	1.27	1.67	3.00	1.17	1.63	Y	Y	12.85	17.98	34.62	0.29

4/16/23 21:35	4/17/23 0:10	1.27	1.30	1.61	1.15	1.32	N	Y	17.56	21.83	36.53	0.52
4/20/23 4:10	4/20/23 6:05	1.27	1.96	2.88	1.07	1.40	N	Y	2.80	3.97	8.79	0.22
4/20/23 13:35	4/20/23 15:45	1.27	1.40	1.63	1.22	0.81	N	Y	5.53	7.16	11.95	
4/21/23 15:30	4/21/23 18:40	1.27	1.35	1.50	1.04	0.58	N	Y	2.02	2.60	4.26	0.17
4/21/23 23:25	4/22/23 0:50	1.27	1.37	1.45	1.27	1.00	N	Y	19.50	24.74	41.81	0.49
4/24/23 20:15	4/24/23 21:35	1.27	1.54	1.88	1.36	1.30	N	Y	6.78	8.84	15.98	0.27
4/27/23 13:15	4/27/23 14:45	1.27	1.61	3.07	0.96	1.52	Y	Y	1.97	2.63	4.85	0.21
4/27/23 21:55	4/28/23 0:35	1.27	1.39	1.58	1.27	2.11	N	Y	13.47	17.48	29.26	0.41
4/29/23 6:10	4/29/23 7:30	1.27	1.79	2.59	1.29	1.58	N	Y	1.19	1.65	3.31	0.16
4/30/23 18:50	4/30/23 21:55	1.27	1.41	1.71	1.19	2.13	N	Y	2.71	3.46	5.92	0.19
5/3/23 0:00	5/3/23 2:00	1.27	1.63	3.04	1.25	1.75	Y	Y	10.98	15.04	29.56	0.30
5/7/23 19:00	5/7/23 21:50	1.27	1.32	1.40	1.24	1.61	N	Y	7.89	10.02	16.42	0.57
5/9/23 5:10	5/9/23 6:15	1.27	2.07	3.36	1.10	1.52	Y	Y	12.19	18.79	42.54	0.33
5/10/23 4:20	5/10/23 5:55	1.27	2.09	3.48	1.29	1.59	Y	Y	8.82	13.62	34.44	0.47
5/18/23 3:30	5/18/23 0:10	1.27	1.41	1.71	1.23	1.73	Y	Y	10.54	13.63	23.19	0.37
6/1/23 4:50	6/1/23 6:00	1.27	2.06	2.72	1.33	1.60	Y	Y	10.71	15.56	35.23	0.21
6/1/23 7:05	6/1/23 7:25	1.27	2.31	2.62	1.55	1.53	Y	Y	8.32	12.62	31.29	0.20
6/2/23 4:50	6/2/23 5:45	1.27	1.60	2.09	1.35	1.48	Y	Y	20.93	28.72	51.93	0.40

6/26/23 5:30	6/26/23 7:25	1.27	1.80	3.16	1.10	1.14	Y	Y	5.21	7.84	16.62	0.30
7/2/23 0:30	7/2/23 3:25	1.27	1.31	1.41	1.20	1.54	N	Y	7.94	9.88	16.43	0.54
7/4/23 20:05	7/4/23 22:35	1.27	1.44	1.83	1.03	1.86	Y	Y	10.25	13.05	23.30	0.44

Table 3: Local BB event (<1 hr)

Start	End	AAE Threshold	Average AAE	Max AAE	Min AAE	SAE	Smoke Overhead	BT through smoke	Absorption coefficient Red	Absorption coefficient Green	Absorption coefficient Blue	Average HCN (ppbv)
4/10/23 23:40	4/10/23 23:55	1.27	2.23	2.73	1.76	1.94	Y	Y	13.2	20.9	47.8	0.17
4/11/23 18:10	4/11/23 18:30	1.27	1.82	2.58	1.41	1.99	Y	Y	4.1	5.8	11.7	0.12
4/12/23 20:35	4/12/23 20:55	1.27	1.75	1.98	1.45	1.14	Y	Y	14.1	19.4	37.8	NaN
4/13/23 5:20	4/13/23 5:25	1.27	1.89	2.04	1.74	1.43	Y	Y	8.2	11.4	23.6	NaN
4/13/23 6:15	4/13/23 6:50	1.27	1.59	1.87	1.25	1.14	Y	Y	19.7	26.4	48.3	NaN
4/14/23 4:35	4/14/23 4:50	1.27	1.74	1.89	1.54	1.45	Y	Y	11.3	15.9	30.2	0.30
4/18/23 9:35	4/18/23 10:15	1.27	1.41	2.17	0.83	0.98	Y	Y	3.8	4.8	8.4	0.16
4/19/23 4:25	4/19/23 4:55	1.27	2.35	2.67	2.08	0.55	N	Y	2.6	3.8	9.4	0.17
4/20/23 6:50	4/20/23 7:35	1.27	1.65	2.13	1.19	0.87	N	Y	4.2	5.6	10.6	0.25
4/23/23 22:50	4/23/23 22:55	1.27	1.63	1.64	1.62	1.85	N	Y	8.7	11.2	21.3	0.26

4/25/23 7:25	4/25/23 7:55	1.27	1.75	2.27	1.54	1.84	N	Y	7.4	10.0	19.7	0.30
4/26/23 4:55	4/26/23 4:55	1.27	2.04	2.04	2.04	1.96	N	Y	8.0	11.5	24.8	0.23
4/26/23 5:50	4/26/23 5:50	1.27	1.75	1.75	1.75	2.00	N	Y	6.0	8.3	16.1	0.19
4/27/23 7:35	4/27/23 7:45	1.27	2.49	2.72	2.30	1.89	Y	N	1.9	2.9	7.5	0.22
4/27/23 11:40	4/27/23 11:40	1.27	2.23	2.23	2.23	1.68	Y	N	1.4	2.0	4.7	0.18
5/1/23 19:20	5/1/23 19:30	1.27	1.83	1.98	1.70	1.25	Y	Y	7.4	10.5	20.8	0.33
5/3/23 20:45	5/3/23 20:55	1.27	2.37	2.72	2.03	1.79	Y	Y	10.0	16.3	39.0	0.27
5/4/23 4:05	5/4/23 4:40	1.27	1.60	2.12	1.38	1.83	Y	Y	10.9	14.9	27.0	0.33
5/4/23 7:40	5/4/23 8:20	1.27	1.55	1.66	1.39	1.57	Y	Y	11.0	14.5	26.1	0.34
5/8/23 6:10	5/8/23 6:40	1.27	2.30	3.08	1.41	1.67	Y	Y	4.9	8.3	18.9	0.56
5/10/23 22:05	5/10/23 22:45	1.27	1.51	1.76	1.34	1.41	Y	Y	5.5	7.5	12.9	0.64
5/11/23 0:00	5/11/23 0:20	1.27	1.57	2.43	1.28	NaN	Y	Y	0.8	1.0	1.8	0.60
5/12/23 4:35	5/12/23 4:40	1.27	1.50	1.52	1.49	1.34	Y	Y	7.2	9.3	16.6	0.42
5/14/23 22:05	5/14/23 22:55	1.27	1.51	1.63	1.38	1.61	N	Y	14.4	18.5	33.2	0.51
5/15/23 20:35	5/15/23 21:15	1.27	1.88	2.17	1.51	1.66	Y	Y	2.7	3.6	7.7	0.41
5/16/23 21:05	5/16/23 21:35	1.27	1.87	2.29	1.59	2.04	Y	Y	2.8	3.9	8.0	0.30
5/18/23 16:40	5/18/23 17:05	1.27	2.34	2.91	1.51	2.19	Y	Y	5.8	9.2	23.2	0.39
5/22/23 21:15	5/22/23 21:35	1.27	1.69	1.81	1.49	1.56	Y	Y	14.2	19.7	36.5	0.52
5/22/23 21:15	5/22/23 21:35	1.27	1.69	1.81	1.49	1.56	Y	Y	14.2	19.7	36.5	0.52
5/25/23 23:15	5/26/23 0:00	1.27	1.83	2.36	1.38	1.48	Y	Y	19.3	24.9	54.6	0.80

5/26/23 21:00	5/26/23 21:25	1.27	1.64	1.82	1.42	1.40	Y	Y	21.6	28.6	54.3	0.72
5/31/23 4:20	5/31/23 4:45	1.27	1.78	2.57	1.27	1.63	Y	Y	15.4	21.7	43.3	0.27
6/1/23 2:45	6/1/23 3:00	1.27	1.75	2.14	1.35	1.55	Y	Y	12.3	17.2	33.2	0.17
6/1/23 3:10	6/1/23 3:25	1.27	1.61	1.91	1.33	1.55	Y	Y	11.7	15.6	28.8	0.17
6/1/23 6:55	6/1/23 7:25	1.27	2.08	2.62	1.35	1.55	Y	Y	8.1	11.8	27.4	0.20
6/1/23 22:30	6/1/23 22:50	1.27	1.94	2.33	1.41	1.50	Y	Y	19.2	27.6	58.3	0.43
6/2/23 2:30	6/2/23 2:40	1.27	1.57	1.83	1.38	1.62	Y	Y	13.1	17.5	31.7	0.26
6/2/23 3:25	6/2/23 3:45	1.27	1.75	2.08	1.37	1.57	Y	Y	16.0	22.3	42.8	0.30
6/6/23 6:40	6/6/23 7:35	1.27	1.65	2.08	1.30	1.58	Y	Y	27.9	37.8	72.8	0.19
6/7/23 6:00	6/7/23 6:30	1.27	1.61	1.98	1.24	1.45	Y	Y	19.1	25.3	47.6	0.27
6/9/23 5:30	6/9/23 6:10	1.27	1.50	1.98	1.11	1.53	Y	Y	25.2	32.9	58.5	0.51
6/10/23 4:40	6/10/23 4:55	1.27	1.95	2.16	1.72	1.93	Y	Y	7.4	10.6	22.3	0.29
6/15/23 4:20	6/15/23 5:00	1.27	1.69	2.22	1.39	1.11	Y	Y	19.6	27.2	51.2	0.48
6/16/23 5:00	6/16/23 5:10	1.27	1.64	1.88	1.46	1.33	Y	Y	2.7	3.7	6.9	0.33
6/16/23 19:55	6/16/23 20:15	1.27	0.94	1.03	0.71	1.43	Y	Y	5.3	6.5	9.1	0.29
6/23/23 19:55	6/23/23 20:15	1.27	1.73	2.07	1.39	1.67	Y	Y	5.8	8.2	15.5	0.39
6/23/23 22:45	6/23/23 22:50	1.27	1.87	1.87	1.86	1.73	Y	Y	7.3	10.3	20.6	0.33
6/24/23 6:45	6/24/23 6:55	1.27	1.55	1.77	1.31	1.57	Y	Y	14.8	19.9	35.4	0.56
6/27/23 6:50	6/27/23 7:15	1.27	1.67	1.93	1.48	1.29	Y	Y	5.4	7.2	13.8	0.32
6/30/23 20:50	6/30/23 20:55	1.27	1.83	1.91	1.75	1.64	Y	Y	5.9	8.3	16.5	0.33
7/5/23 4:35	7/5/23 5:20	1.27	2.33	2.75	1.65	1.73	Y	Y	3.7	5.5	13.9	0.28
7/6/23 5:30	7/6/23 6:30	1.27	1.45	2.71	1.14	0.68	Y	Y	10.4	13.3	22.5	0.36

Appendix C. Finalized Datasets

The following HCN data files accompany this report:

- HCNatBC2_ARIdata_*yyyymmdd*.txt
- HCNatBC2_ARIdata_Readme_*yyyymmdd*.txt
- HCNatBC2_5min_ARIdata_*yyyymmdd*.txt
- HCNatBC2_5min_ARIdata_Readme_*yyyymmdd*.txt

They have been submitted to the AQRP and are available for download at:

https://herndon.homeunix.net/owncloud/index.php/s/T2sQjLcqykmEllC